

**TOWARD THE CRYSTAL STRUCTURE OF A TYPE III ANTIFREEZE  
PROTEIN FROM OCEAN POUT, *MACROZOARCES AMERICANUS***

By

**STEVEN A. BUBANKO, B.Sc.**

A Thesis

Submitted to the School of Graduate Studies

in Partial Fulfillment of the Requirements

for the Degree

Master of Sciences

McMaster University

© Copyright by Steven Bubanko, August 1996

MASTER OF SCIENCE (1996)

(Biochemistry)

McMASTER UNIVERSITY

Hamilton, Ontario

**TITLE:** Toward the Crystal Structure of a Type III Antifreeze Protein from Ocean Pout, *Macrozoarces americanus*.

**AUTHOR:** Steven A. Bubanko, B.Sc. (McMaster University)

**SUPERVISOR:** Dr. Daniel S.C. Yang

**NUMBER OF PAGES:** xiii, 82

---

## ABSTRACT

---

Four structurally distinct types of macromolecular antifreezes have been previously isolated from the sera of polar marine fish. When the water temperature surrounding these organisms drops below  $-0.7^{\circ}\text{C}$ , the freezing point of their bodily fluids, any contact with surrounding ice will nucleate internal ice crystal growth. The antifreeze proteins (AFPs) and antifreeze glycoproteins (AFGPs) synthesized by the fish act to inhibit the growth of existing ice crystals in their sera through direct adsorption to the ice lattice. The  $\alpha$ -helical structure of type I AFP from winter flounder has been solved to atomic resolution and its mechanism of ice binding has been proposed. The NMR solution structure of a type III AFP from ocean pout has identified proteins in this class to exist in a  $\beta$ -sandwich conformation, however their mechanism of action remains uncertain.

To facilitate the pursuit of an x-ray crystal structure solution, we subcloned the gene for a type III AFP (HPLC6) into pET15b and expressed recombinant His-rHPLC6 AFP in *E. coli*. Purified rmHPLC6 product has been successfully crystallized, and heavy atom soaks were performed in order to attempt a structure solution by multiple isomorphous replacement. The lone tyrosine in this recombinant AFP has been successfully derivatized in solution with iodine, and the modified protein was crystallized.

In order to optimize the measurement of anomalous scattering information, modifications to our data collection system were required. Cryocrystallography techniques were employed to improve the quality of collected data.

The expression, purification, crystallization and optimized data collection on an iodine-derivatized type III AFP from ocean pout will be presented here. This work has been instrumental in providing the high quality x-ray data required to solve the crystal structure to atomic resolution. Future examination of the solved structure will promote an increased understanding of the ice-binding mechanism exhibited by this class of proteins.

---

## ACKNOWLEDGEMENTS

---

I would like to convey my utmost appreciation to my supervisor, Dr. Daniel S.C. Yang, for providing the guidance and the environment essential to the completion of this work. I would especially like to thank the other members of my Research Committee, Dr. G.D. Wright and Dr. A. Edwards, for their continued assistance and valuable suggestions.

Much gratitude is also extended to Dr. Albert Berghuis for sharing his data processing and computational skills, and for many hours of enlightening conversation during the midnight shift at the NSLS. I thank Dr. G.L. Fletcher for the G75 type III AFP, Dr. C.L. Hew for the  $\lambda$ PCLII-rHPLC6 vector, and Dr. V.S. Ananthanarayanan for the use of his HPLC, all of which were indispensable to the success of this project.

Great thanks are also extended to the members of my laboratory, both past and present, especially Dr. Paul Ala, Dr. Frank Sicheri, Susan Xue and Wai Ching Hon for their scientific input and for making my research experience an enjoyable one. Additional recognition is deserving for Susan Xue due to her valuable assistance in the crystal growing endeavour.

Thanks must be given to my family and friends for their continued patience and valuable support during the course of this work. In closing, I would like to express my deepest gratitude to the editorial committee (Paul Thompson) for ensuring the absence of any spelling mistakes in this manuscript.

I dedicate this work to my family and to the memory of two dear friends,

Brian David Storoni and Walter Rokoss.

*Maybe it's just not good enough to go on like nothing's changed.*

**-The Skydiggers-**

---

## TABLE OF CONTENTS

---

	<b>PAGE</b>
<b>ABSTRACT</b>	<b>iii</b>
<b>ACKNOWLEDGEMENTS</b>	<b>v</b>
<b>TABLE OF CONTENTS</b>	<b>vii</b>
<b>ABBREVIATIONS</b>	<b>x</b>
<b>LIST OF FIGURES</b>	<b>xi</b>
<b>LIST OF TABLES</b>	<b>xiii</b>
<b>CHAPTER ONE: INTRODUCTION</b>	<b>1</b>
1.1 Four Distinct Types of Macromolecular Antifreezes	1
1.2 Function of Macromolecular Antifreezes	4
1.3 Adsorption-Inhibition of Ice Crystal Growth	5
1.4 Molecular Mechanism of the Protein-Ice Interaction	7
1.5 Objectives	9
<b>CHAPTER TWO: TYPE III AFPs FROM OCEAN POUT SERA</b>	<b>16</b>
2.1 Introduction	16
2.2 Crystallization of Ocean Pout Type III AFPs	17

2.3 Data Collection	18
2.4 Reverse Phase and Ion Exchange Chromatography	19
2.5 Discussion	20
<b>CHAPTER THREE: OCEAN POUT HPLC6 AFP FROM <i>E. COLI</i></b>	<b>26</b>
3.1 Introduction	26
3.2 Purification of rmHPLC6 Using the pET His-tag <sup>®</sup> System	27
3.2.1 <i>Construction of the pET15b-rHPLC6 vector</i>	27
3.2.2 <i>Expression of His-rHPLC6 type III AFP</i>	28
3.2.3 <i>Purification procedure</i>	28
3.3 Thermal Hysteresis Activity Assay	31
3.4 Discussion	32
<b>CHAPTER FOUR: rmHPLC6 CRYSTALS, DERIVATIVES AND DATA COLLECTION</b>	<b>44</b>
4.1 Crystallization of rmHPLC6 Type III AFP	44
4.2 Additional Cloning Experiments	45
4.3 Preparation of Heavy Atom Derivatives	47
4.3.1 <i>Crystal soaking</i>	47
4.3.2 <i>Cross-linking with gluteraldehyde</i>	48
4.3.3 <i>Iodination of rmHPLC6 in solution</i>	49
4.3.4 <i>Selenomethionyl rmHPLC6</i>	50
4.4 Cryocrystallographic Data Collection	51
4.5 Discussion	52

<b>CHAPTER FIVE: CONCLUSION</b>	<b>67</b>
<b>GLOSSARY</b>	<b>69</b>
<b>REFERENCES</b>	<b>70</b>

---

## ABBREVIATIONS

---

Å	=	Ångstrom
AFGP	=	antifreeze glycoprotein
AFP	=	antifreeze protein
CD	=	circular dichroism
cDNA	=	complementary DNA
DNA	=	deoxyribonucleic acid
E. coli	=	Escherichia coli
HPLC	=	high performance liquid chromatography
LB-amp	=	Luria-Bertani Broth supplemented with 0.5 µg/ml ampicillin
MPD	=	2-methyl-2,4-pentanediol
NEB	=	New England Biolabs
NMR	=	nuclear magnetic resonance
OD	=	optical density
PCR	=	polymerase chain reaction
PEG	=	polyethylene glycol
rHPLC6	=	MK-HPLC6-K
rmHPLC6	=	GSHMK-HPLC6-K
SDS-PAGE	=	sodium dodecyl sulfate polyacrylamide gel electrophoresis

---

## LIST OF FIGURES

---

<b>FIGURE</b>	<b>TITLE</b>	<b>PAGE</b>
1.1	The four types of macromolecular antifreezes	11
1.2	Schematic representations of a hexagonal ice crystal, $I_h$	12
1.3	Concentration dependence of typical antifreeze activity profiles	13
1.4	Inhibition of a growing ice front by adsorbed AFPs	14
1.5	Winter flounder AFP ice binding model	15
2.1	Reverse phase purification of G75 type III AFP	21
2.2	Sequence homology exhibited by type III AFPs	22
2.3	Elution profile from Xue <i>et al.</i> , 1994	23
2.4	Schematic of G75 type III AFP reverse phase purification	24
2.5	Schematic of G75 type III multiple-column purification	25
3.1	Amino acid sequences of native and recombinant ocean pout HPLC6	35
3.2	Construction of the pET15b-rHPLC6 vector	36
3.3	rmHPLC6 purification summary	37
3.4	Reverse phase purification of the thrombin cleavage reaction products	38
3.5	Reverse phase profile of rmHPLC6 type III AFP	39

3.6	Thermal hysteresis activity assay	40
3.7	rmHPLC6 standard curve	41
3.8	A comparison of thermal hysteresis curves for fish AFPs and AFGPs	42
4.1	Initial crystals of rmHPLC6	57
4.2	Diffraction quality crystal of rmHPLC6	58
4.3	Amino acid sequences of HPLC6, rmHPLC6 and eHPLC6	59
4.4	A damaged rmHPLC6 crystal	60
4.5	Reverse phase purification of iodinated rmHPLC6	61
4.6	Mass spectral profiles of rmHPLC6 iodination products	62
4.7	Crystals of mono-iodinated rmHPLC6	63
4.8	Crystals of selenomethionyl rmHPLC6	64
4.9	Modified “cryo box”.	66
5.1	2.0 Å X-ray crystal structure of a type III AFP from ocean pout	68

---

## LIST OF TABLES

---

<b>TABLE</b>	<b>TITLE</b>	<b>PAGE</b>
1.1	Four distinct types of macromolecular antifreezes from polar marine fish	10
2.1	Crystallization conditions for serum-purified ocean pout AFPs	18
3.1	Purification table for rmHPLC6	43
4.1	Data collection summary	65

## **CHAPTER ONE:**

---

# **INTRODUCTION**

---

### **1.1 Four Distinct Types of Macromolecular Antifreezes**

Many organisms on earth are often faced with a situation in which the temperature of the surrounding environment can drop below the freezing point of their internal fluids. In response to this situation, these animals must either relocate to a warmer environment or possess a survival mechanism which challenges the threat of freezing to death. This is particularly apparent for polar marine fish living off the Newfoundland coast where the winter temperature of the North Atlantic ocean drops to around  $-1.9^{\circ}\text{C}$ , yet the sera of these fish will freeze at  $-0.7^{\circ}\text{C}$  (Holmes & Donaldson, 1969). To protect themselves from their harsh environment, the fish synthesize proteinaceous macromolecular antifreezes which function to prevent their bodily fluid from freezing (reviewed in Feeney & Yeh, 1978; DeVries, 1983; Feeney, Burcham & Yeh, 1986; Ananthanarayanan, 1989; Davies & Hew, 1990; Hew & Yang, 1992; Yang, 1993).

Four distinct types of macromolecular antifreezes have been isolated from marine teleosts as outlined in Table 1.1 (reviewed in Ananthanarayanan, 1989; Davies & Hew, 1990; Hew & Yang, 1992; Yang, 1993). The antifreeze glycoproteins (AFGPs) each possess carbohydrate groups and thus represent the first class of macromolecular antifreezes. They are found in different species of cod (DeVries & Wohlschlag, 1969; Hew *et al.*, 1981) and are comprised of a repeating tripeptide unit of Ala-Ala-Thr with the disaccharide  $\beta$ -D-galactosyl-(1 $\rightarrow$ 3)- $\alpha$ -N-acetyl-D-galactosamine linked to the threonine residue (Feeney & Yeh, 1978). Tripeptide repeats of up to 50 units generate AFGPs ranging in size from 2.6 to 33 kDa (DeVries, Komatsu & Feeney, 1970). CD (Ananthanarayanan, 1989) and NMR (Bush & Feeney, 1986; Rao & Bush, 1987) studies have corroborated the most plausible AFGP structural model which has the polypeptide backbone folding into a polyproline II-like left-handed helix with three residues per turn (Franks & Morris, 1978; Bush *et al.*, 1981).

The remaining three classes of antifreeze polypeptides (AFPs) are distinguished on the basis of considerable sequence and structural diversity. Type I AFPs are 3.3 to 6.0 kDa alanine-rich polypeptides which have been isolated from species of flounder (Duman & DeVries, 1976) and sculpin (Hew, Fletcher & Ananthanarayanan, 1980). The recent three-dimensional x-ray crystallographic solution of a flounder AFP to 1.5Å (Yang *et al.*, 1988; Sicheri & Yang, 1995) has shown that type I AFPs exist as lone  $\alpha$ -helices, thus confirming the results from initial low temperature CD studies (Ananthanarayanan & Hew, 1977).

Cystine-rich type II AFPs have been isolated from sea raven (Slaughter *et al.*, 1981; Ng, Trinh & Hew, 1986), smelt and herring (Ewart & Fletcher, 1990) with

approximate masses of 13 to 17 kDa. Other cystine-rich proteins possessing antifreeze activity have been isolated from insects, however additional information is required before they can be classified as type II AFPs (Schneppenheim & Theede, 1980; Patterson & Duman, 1981; Hew *et al.*, 1983). Low temperature CD spectral data and structure prediction methods have assigned the presence of  $\beta$ -structure (Slaughter *et al.*, 1981; Ng, Trinh & Hew, 1986). Type II AFPs have also been found to share 20% sequence homology with the carbohydrate-recognition domain of calcium dependent (C-type) lectins, making them the only class of AFPs which exhibits homology with other proteins (Ng & Hew, 1992; Ewart, Rubinsky & Fletcher, 1992; Ewart & Fletcher, 1993). The three-dimensional structures of two C-type carbohydrate-recognition domains have been solved (Weis *et al.*, 1991, 1992; Graves *et al.*, 1994). In particular, the domain from a rat mannose-binding protein (Weis *et al.*, 1992) has provided a basis for the generation of a structural model of type II AFP from sea raven using comparative modeling techniques (Sonnichsen, Sykes & Davies, 1995). This structure predicts the presence of two  $\alpha$ -helices and two  $\beta$ -sheets in the type II AFP.

Type III AFPs were first isolated from the Newfoundland ocean (eel) pout, *Macrozoarces americanus* (Hew *et al.*, 1984), and subsequently from Antarctic pout (Schrag *et al.*, 1987; Wang, DeVries & Cheng, 1995), Arctic pout (Cheng & DeVries, 1989), and wolffish (Scott *et al.*, 1988). They have been identified as lacking any abundance of alanine or cystine and thus were determined to represent a third class of AFPs. Purification of Newfoundland ocean pout sera through Sephadex G75 and C18 reverse phase columns has resolved up to twelve distinct type III AFPs all between 5.7 and 7 kDa in size (Hew *et al.*, 1984). Sequencing of the major component AFPs identified amino acid differences that could only be the products of multiple genes rather than post-

translational modifications (Hew *et al.*, 1988). In 1993, the solution structure of HPLC 12 was determined by NMR spectroscopy (Sonnichsen *et al.*, 1993). It differs from the structures all other macromolecular antifreezes such that this structure consists of two sheets of three antiparallel strands and one sheet of two antiparallel strands, with the triple-stranded sheets forming a  $\beta$ -sandwich (Figure 1.1).

## 1.2 Function of Macromolecular Antifreezes

Under normal conditions, water crystallizes at 0°C and 1 atmosphere pressure in a hexagonal space group (Figure 1.2). This is the most common form of ice and is referred to as  $I_h$  (Fletcher, 1970; Hobbs, 1974). At temperatures above -4°C, normal ice growth occurs on the prism faces of ice producing circular disks. Generally, raising or lowering the temperature by 0.01°C induces either melting or freezing respectively, therefore the melting and freezing points are taken to be the same (DeVries, 1983).

In shallow coastal waters contact with ice is unavoidable, therefore at temperatures below -0.7°C, ice crystals will form in the sera of marine teleosts. However, the uninhibited freezing of fish body fluids is always fatal (Scholander *et al.*, 1957) due to both osmotic damage resulting from dehydration and physical damage caused by ice crystal formation (Feeney & Yeh, 1978). Despite being structurally, immunologically and compositionally distinct, each of the four types of macromolecular antifreezes all perform the same function: to adsorb to the surface of growing ice crystals and subsequently inhibit further ice growth. This noncolligative act of freezing point depression is called thermal hysteresis (DeVries, 1971; Scholander & Maggert, 1971; Feeney & Hofmann, 1973; Raymond & DeVries, 1977). Antifreeze activity is defined as the extent of

hysteresis in °C afforded by the AFPs and AFGPs. Figure 1.3 illustrates the discrepancy between the relatively unchanged melting temperature and the AFP-depressed freezing temperature. At low protein concentrations, antifreeze activity is proportional on a near linear scale, however at physiological concentrations of 20 to 40 mg/ml (Ananthanarayanan, 1989) the activity becomes saturated, with the more effective antifreeze proteins providing over 1°C of protection (DeVries, 1983; Davies & Hew, 1992)

### **1.3 Adsorption-Inhibition of Ice Crystal Growth**

The pursuit of elucidating a mechanism of action common to the different macromolecular antifreezes has involved many interesting and elegant experiments. Upon microscopic observation of ice crystals grown in the presence of AFPs and AFGPs, it became apparent that preferential interaction with specific ice planes is responsible for altering the morphology of growing ice crystals. Ice growth along the basal plane is hindered while growth parallel to the *c* axis becomes prominent, producing fine needles instead of normal dendritic ice (Scholander & Maggert, 1971; Raymond & DeVries, 1977; Knight, DeVries & Oolman, 1984; Harrison *et al.*, 1987; Chao, DeLuca & Davies, 1995). Also significant was the finding that unlike most proteins and solutes, normally excluded from a growing ice front, antifreeze proteins adsorb to the ice surface and are incorporated into the ice phase. This result, first discovered by measuring the transition temperature of a freezing event (Raymond & DeVries, 1972), was later confirmed by Raman spectroscopy (Tomimatsu *et al.*, 1976), light spectroscopy in combination with surface second harmonic generation (Brown *et al.*, 1985), and freeze etching (Knight, Cheng & DeVries, 1991; Knight, Driggers & DeVries, 1993).

An explanation of thermal hysteresis requires one to address the paradox of how antifreeze adsorption to ice depresses the freezing point yet leaves the melting temperature unaffected. Knight and DeVries developed an interesting experiment in which they melted the inside of 60 cm<sup>3</sup> ice crystals to create “negative crystals” (Knight & DeVries, 1989). They concluded that adsorbed AFGPs could inhibit melting in the same manner in which they inhibit freezing, although melting inhibition was found to only occur on concave ice faces. Since ice crystals in nature express only convex ice faces, melting inhibition is not normally observed. Therefore the melting temperature remains largely unchanged despite the presence of AFPs and AFGPs.

Two theories have been proposed to account for the inhibition of ice growth by macromolecular antifreezes. The first is the “adsorption-inhibition” theory which, based on the Kelvin Effect, evaluates the thermodynamic consequences of antifreeze proteins adsorbing to ice (Raymond & DeVries, 1977; Knight, Cheng & DeVries, 1991). Simply, as ice continues to grow between adsorbed protein molecules, the surface curvature of the ice front increases to a point where further freezing becomes energetically unfavourable (Figure 1.4). This model relies on a relative permanence of the protein-ice interaction. The second theory considers kinetic properties which assume a reversible binding equilibrium (Yang, 1993). In this situation, antifreeze proteins are competing with water molecules during the freezing process, therefore any adsorbed AFPs act as a kinetic barrier to growth. In support of this theory, Burcham *et al.* observed that as the concentration of AFGP is increased, the growth rate of ice slows, eventually to a point where ice growth is completely inhibited by sufficiently high protein concentrations (Burcham *et al.*, 1986).

## 1.4 Molecular Mechanism of the Protein-Ice Interaction

Despite the kinetic and thermodynamic theories explaining the inhibition of ice growth by adsorbed proteins, a true understanding of the molecular mechanism of protein-ice interaction can only be obtained via high resolution structural information. Currently only one of the four macromolecular antifreezes is characterized by a structural solution to atomic resolution, the  $\alpha$ -helical type I AFP from winter flounder (Yang *et al.*, 1988; Sicheri & Yang, 1995). Hydrophilic residues such as threonine, asparagine, and aspartic acid are located on one side of the “pseudo” amphipathic helix, thus presenting a flat polar surface for interaction with ice. The recently-solved 1.5Å crystal structure (Sicheri & Yang, 1995) revealed these polar residues to exist as components in two conserved ice-binding motifs, Thr-Asn-Leu and Thr-Asp-Lys. The Leu and Lys residues were found to be critical in restraining the torsional motion of the Asp and Asn side chains so as to provide a rigid framework of hydrogen bonds for ice binding. Based on their structure, Sicheri & Yang proposed that the polar residues of type I AFP adsorb to the ice lattice ridges, in contrary to earlier theories which suggested these amino acids intercalate directly into the growing ice face (Wen & Laursen, 1992; Knight, Driggers & DeVries, 1993). Freeze etching techniques identified the  $\{20\bar{2}1\}$  pyramidal ice plane as the preferential site of binding for winter flounder AFP, as shown in Figure 1.2 (Knight, Cheng & DeVries, 1991). More specifically, they determined the AFP to align along the  $\langle 01\bar{1}2 \rangle$  binding axis of ice (Figure 1.5). In this direction, the ice lattice repeat distance of 16.7Å corresponds with the distance between the ice-binding residues along the AFP  $\alpha$ -helix (Knight, Cheng & DeVries, 1991; Sicheri & Yang, 1995).

In comparison, much less is known of the AFGPs' and type II AFPs' mechanism of action. As a polyproline II-like left-handed helix with three residues per turn, the AFGPs

adopt an amphipathic helix similar to the type I AFP (Franks & Morris, 1978; Bush *et al.*, 1981). Freeze etching was used to identify ice prism planes as the preferred binding site for AFGPs 7 and 8, again due to the matching of repeat distances between AFGP disaccharide hydroxyls and the ice lattice (Ananthanarayanan, 1989; Knight, Driggers & DeVries, 1993). As for the type II AFPs, the recent structural model proposes a binding site in the region of the triple stranded  $\beta$ -sheet (Sonnichsen, Sykes & Davies, 1995), however a structure solution to atomic resolution will be essential to confirm this hypothesis.

As for the type III AFPs from ocean pout, the successful expression and purification of both HPLC6 (Li, Trinh & Hew, 1991) and HPLC12 (Chao *et al.*, 1993) has permitted an investigation of the ice-binding mechanism via site-directed mutagenesis. Li and Hew have implicated two conserved glutamic acid residues as contributors to the thermal hysteresis activity of HPLC6 (Li & Hew, 1991). Using the NMR structure of HPLC12 (Sonnichsen *et al.*, 1993) and sequence alignment information, Chao *et al.* identified a cluster of conserved, surface accessible polar amino acids on the C-terminal  $\beta$ -sheet (Chao *et al.*, 1994). Since the mutant HPLC12 type III AFPs were correctly folded, the reduction in thermal hysteresis observed with several mutants suggested these residues play a role in ice-binding. However, the above information fails to produce an exact molecular mechanism of ice binding by the type III AFPs. An x-ray crystal structure solution to atomic resolution will be essential to this pursuit.

## **1.5 Objectives**

The structure of an  $\alpha$ -helical type I AFP from winter flounder has been solved to atomic resolution, and its molecular mechanism for ice binding has been proposed (Sicheri & Yang, 1995). The complete characterization of the structure and function of a globular type III AFP from ocean pout is paramount in order to propose a general mechanism by which proteins interact with ice. This information will have much potential impact on future research into supercooling and cryobiology.

**Table 1.1: Four distinct types of macromolecular antifreezes from polar marine fish.**

	<u>AFGP</u>	<u>Type I AFP</u>	<u>Type II AFP</u>	<u>Type III AFP</u>
<b>Feature:</b>	carbohydrate rich	alanine rich	cystine-rich	average
<b>M<sub>r</sub>:</b>	2.6 - 33 kDa	3.3 - 6 kDa	13 - 17 kDa	5.7 - 7 kDa
<b>Fish Species:</b>	Antarctic cod Atlantic cod Greenland Cod Polar cod Saffron Cod	Winter flounder Yellowtail flounder Arctic sculpin Shorthorn sculpin Grubby sculpin Alaskan Plaice	Sea raven Smelt Herring	Ocean pout Wolffish Antarctic pout Arctic pout
<b>AFP Production:</b>	30 - 40 mg/ml all year	> 20 mg/ml seasonal	> 20 mg/ml seasonal	20 - 25 mg/ml all year
<b>Primary Structure:</b>	(Ala-Ala-Thr) <sub>n</sub> disaccharide	11 amino acid repeat	disulfide- linked	average
<b>Secondary Structure:</b>	polyproline II LHD helix (CD, NMR)	amphipathic α-helical (CD, X-ray)	β-sheet & α-helix (CD, NMR, modelling)	β-sandwich (CD, NMR)
<b>Diagrams:</b>	<p><math>[-\text{Ala}-\text{Ala}-\text{Thr}-]_n</math></p>			

Figures reproduced from Davies & Hew, 1990.

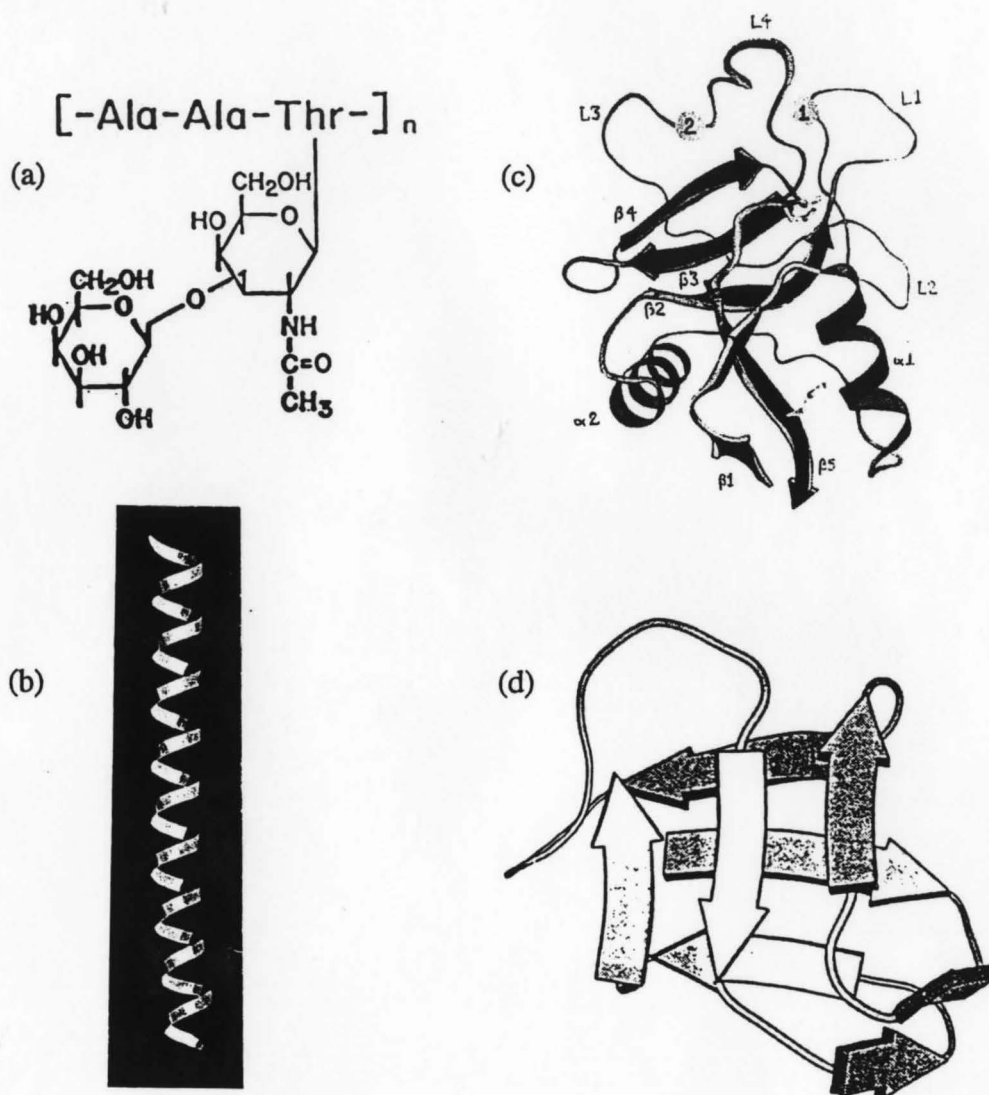


**Figure 1.1: The four types of macromolecular antifreezes.** (a) Ala-Ala-Thr-disaccharide repeating motif found in AFGPs (suggested to form a secondary structure similar to a left-handed polyproline II helix). Reproduced from Davies & Hew, 1990. (b) X-ray structure of type I AFP from winter flounder. Reproduced from Sicheri & Yang, 1995. (c) X-ray structure of a carbohydrate-recognition lectin domain (used as the basis for a model of type II AFP from sea raven). Reproduced from Weis *et al.*, 1991. (d) NMR solution structure of HPLC 12, a type III AFP from ocean pout. Reproduced from Sonnichsen *et al.*, 1993.

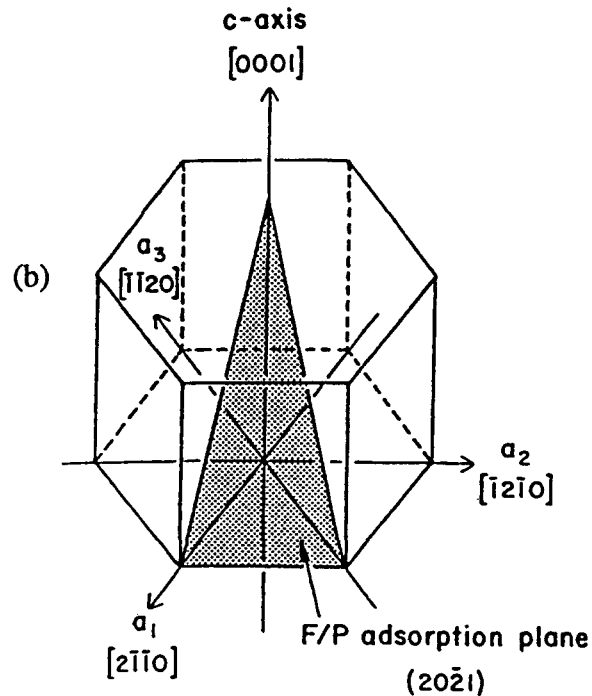
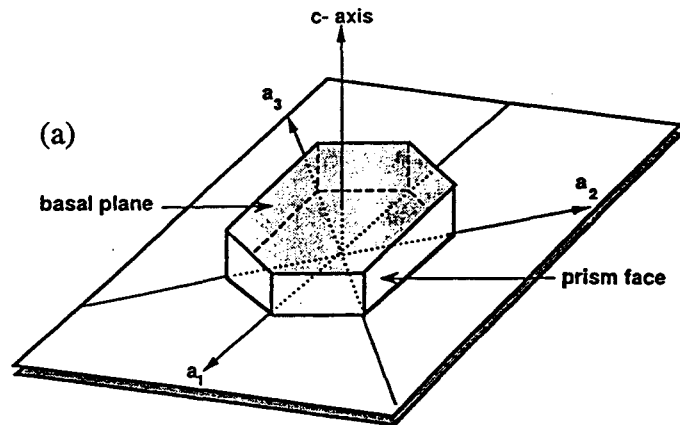


**Figure 1.2: Schematic representations of a hexagonal ice crystal,  $I_h$ .** (a) The basal plane, prism faces, the  $c$  and three  $a$  axes are shown. Normal ice growth occurs on the prism faces producing circular disks. Reproduced from Hew & Yang, 1992. (b) The  $\{20\bar{2}1\}$  pyramidal binding plane of winter flounder type I AFP is illustrated. Reproduced from Knight, Cheng & DeVries, 1991.

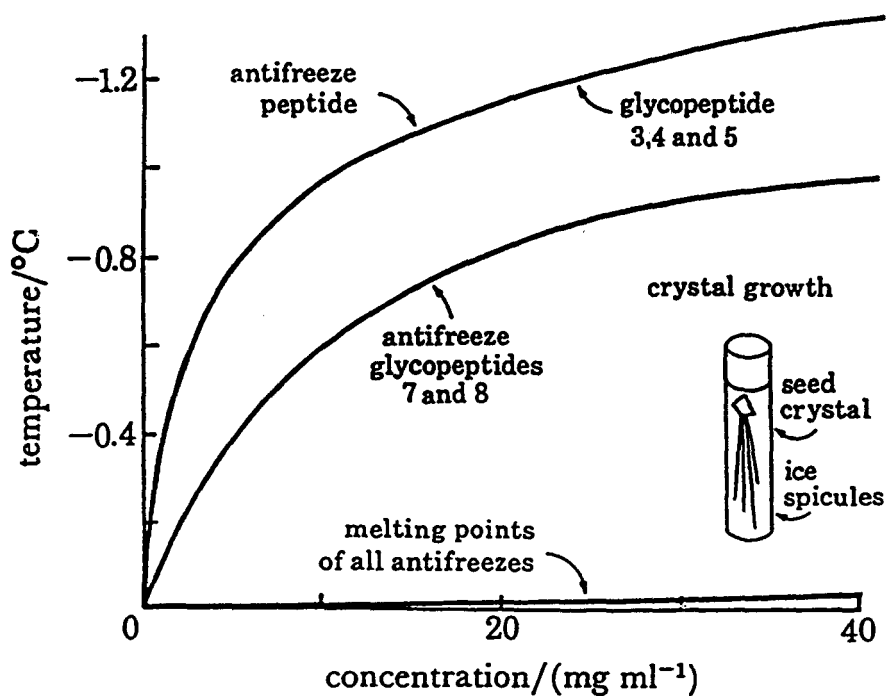


**Figure 1.3: Concentration dependence of typical antifreeze activity profiles.** Macromolecular antifreezes depress freezing points while leaving the melting temperatures unchanged. Melting temperature is the point at which an ice seed crystal melts. Freezing temperature is indicated by the formation of ice spicules from a seed crystal. Reproduced from DeVries, 1984.

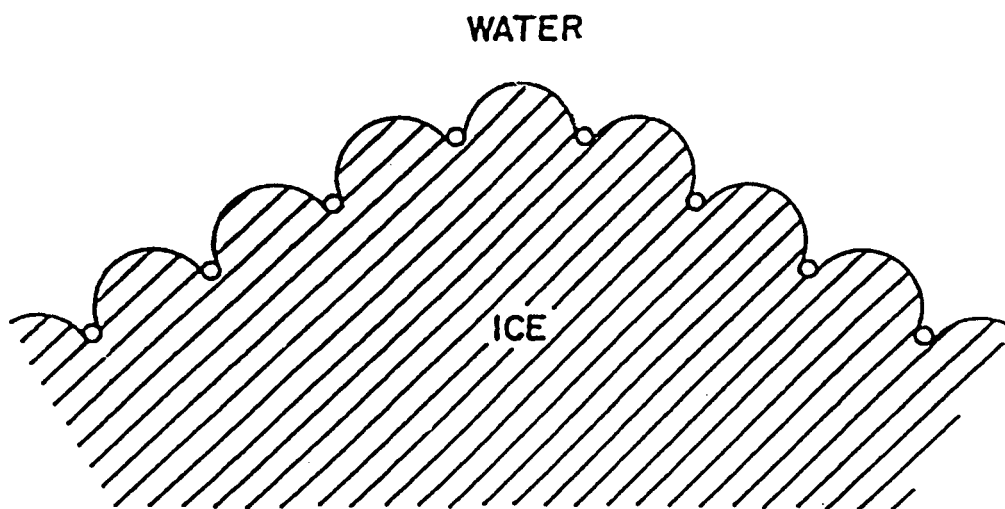


**Figure 1.4: Inhibition of a growing ice front by adsorbed AFPs.** As the ice front grows between the adsorbed AFP molecules (open circles), the increased surface curvature makes additional freezing energetically unfavourable based on the Kelvin Effect. Reproduced from Knight, Cheng & DeVries, 1991.

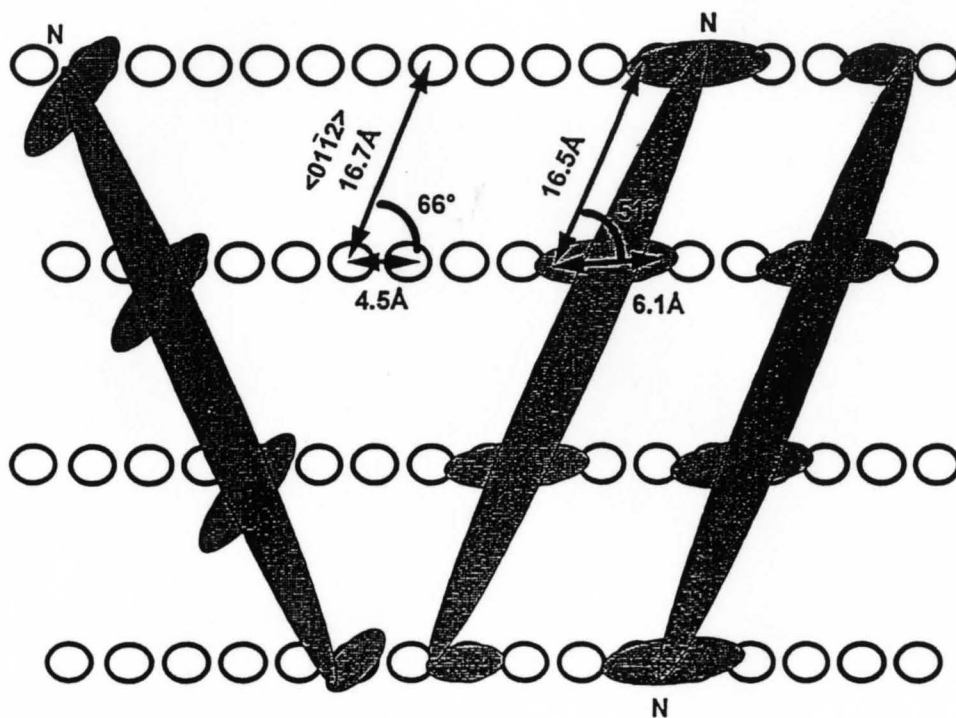


**Figure 1.5: Winter flounder AFP ice binding model.** An illustration of the complementarity between ridges of the  $\{20\bar{2}1\}$  ice plane (open circles) and the type I AFP molecules (shaded). By aligning along the  $\langle 01\bar{1}2 \rangle$  binding axis, the 16.7 Å repeating distance between AFP ice-binding motifs corresponds with the ice lattice periodicity. Reproduced from Sicheri & Yang, 1995.

## **CHAPTER TWO:**

---

# **TYPE III AFPs FROM OCEAN POUT SERA**

---

### **2.1 Introduction**

Unlike kinetic and biochemical protein studies, the trial and error process of crystal growth requires milligram quantities of pure protein in order to maximize the potential for success. Thus, the first obstacle one must overcome in any protein structure determination experiment is to find a plentiful source of crystallizable material. One of the more traditional sources has been via purification of the target protein directly from animal or plant tissue.

Ocean pout were obtained by divers from the waters surrounding the Avalon Peninsula in Newfoundland. Sera was isolated by low speed centrifugation (4000 x g for 15 minutes) and then stored at -20°C (Fletcher, 1977). The pooled serum was dialyzed in 0.1 M  $\text{NH}_4\text{HCO}_3$  using Spectrapor tubing (3.5 kDa cutoff) and clarified by centrifugation before purification through a Sephadex G75 column. Collected fractions were evaluated for antifreeze activity using a freezing point osmometer (Hew, Fletcher &

Ananthanarayanan, 1980) and active fractions were pooled then passed a second time through the G75 column. Again, active fractions were pooled and then lyophilized, generating a stock of G75 type III AFP which was suitable for further purification via ion exchange and reverse phase HPLC (Hew *et al.*, 1984; Li *et al.*, 1985).

As previously mentioned, initial studies on ocean pout sera revealed the presence of twelve individual type III AFPs, each between 5.7 and 7.0 kDa in size. Based on ion exchange binding properties, sequence homology, and immunological cross-reactivity, they are classified into two distinct groups (Hew *et al.*, 1984; Li *et al.*, 1985; Hew *et al.*, 1988). The larger group is comprised of the first eleven peaks to elute off a C18 reverse phase column (Figure 2.1), all of which bind to SP-Sephadex (cation exchange), and exhibit 90% sequence homology with each other (Figure 2.2). The remaining AFP, HPLC12, represents the second group due to its affinity for QAE-Sephadex (anion exchange), and its only 50% sequence homology with the proteins of group one (Hew *et al.*, 1984; Li *et al.*, 1985; Hew *et al.*, 1988).

## 2.2 Crystallization of Ocean Pout Type III AFPs

In 1993, the G75 type III AFP was purified in our laboratory using a Waters  $\mu$ Bondapak C18 column (7.8 mm x 30 cm) (Waters, Mississauga, ON) and a 40 minute acetonitrile gradient of 30% to 50% in 0.1% trifluoroacetic acid and H<sub>2</sub>O. This step resolved the twelve type III AFPs into five major peaks (Figure 2.3) which were subsequently collected, lyophilized and used for crystallization trials (Xue *et al.*, 1994). The component AFPs in each of the five peaks are outlined in Figure 2.4. Each peak was resuspended in 0.1 M Tris-HCl pH 7.1 and screened using the hanging drop vapour

diffusion method with Hampton Crystal Screen I (Hampton Research, Riverside, CA). Peaks 1 and 3 yielded crystals on the initial screen and diffraction quality crystals (0.3mm x 0.05mm x 0.9mm)\* were generated at 4°C over seven weeks in drops with 5 µl of a 20 mg/ml protein solution and 15 µl of the following crystal screen: 2.0 M ammonium phosphate in 0.1 M Tris-HCl pH 7.1 (Xue *et al.*, 1994). In all cases, supersaturation conditions were induced in the hanging drop via equilibration against a lower well of 0.7 ml of the same crystal screen used to form the hanging drop. Successful crystallization conditions are summarized below:

**Table 2.1: Crystallization conditions for serum-purified ocean pout AFPs.**

<u>Protein</u>	<u>Screen</u>	<u>Salt</u>	<u>Buffer</u>	<u>Precipitant</u>	<u>Morphology</u>
Peak1	1.48	none	0.1 M Tris-HCl pH 8.5	2.0 M NH <sub>4</sub> H <sub>2</sub> PO <sub>4</sub>	Large Rods*
Peak3	1.48	none	0.1 M Tris-HCl pH 8.5	2.0 M NH <sub>4</sub> H <sub>2</sub> PO <sub>4</sub>	Thick Plates
Peaks 1 & 3	1.04	none	0.1 M Tris-HCl pH 8.5	2.0 M NH <sub>4</sub> H <sub>2</sub> PO <sub>4</sub>	Thin Plates

(Crystals marked with an asterisk were used for data collection.)

### 2.3 Data Collection

Data collection was initially performed at 4°C on a RAXIS IIC area detector with CuK $\alpha$  radiation from a Rigaku RU200 rotating anode generator operating at 3kW (60mA x 50kV) with SUPPER double focusing mirrors and a 0.2mm focal spot (Xue *et al.*, 1994). This unit was used for all subsequent data collection presented in this manuscript, therefore only modifications to the above unit will be mentioned henceforth. Crystals were mounted in capillary tubes and three still frames taken at 45° intervals were used by

the RAXIS processing software to determine the space group as  $P2_1$ . The dimensions of the monoclinic unit cell were  $a = 39.77\text{\AA}$ ,  $b = 58.51\text{\AA}$ ,  $c = 30.27\text{\AA}$ , and  $\beta = 102.28^\circ$ , with two 6.5 kDa molecules per asymmetric unit (Xue *et al.*, 1994). Refinement statistics for all x-ray data will be presented in Table 4.1.

## 2.4 Reverse Phase and Ion Exchange Chromatography

Generally, an entirely homogeneous protein sample of high purity is essential to the growth of diffraction quality crystals suitable for x-ray analysis. Even though the above crystals were grown from mixtures of type III AFPs having over 90% sequence homology and conservative amino acid substitutions, an ideal situation would involve crystal growth from a solution containing only a single AFP isoform. In this situation, the amino acid sequence of the crystallized component would be known, thus eliminating uncertainty when the polypeptide chain must be traced through the electron density map in pursuit of a structure solution. Secondly, an increase in sample purity has been proven to be directly correlated with the production of better crystals and therefore, an increased diffraction limit (Giege *et al.*, 1986).

Lyophilized G75 type III AFP was kindly provided by Dr. Choy Hew and Dr. Garth Fletcher. The different affinities of the twelve type III AFPs for anion exchange, cation exchange, and reverse phase columns were exploited in an attempt to individually isolate each AFP, however the co-elution of certain peaks could not be resolved. The purification is summarized in Figure 2.5. Each final product, be it an individual isoform or a group of AFPs, was passed through a C18 column as in Figure 2.1, lyophilized, resuspended to 20 mg/ml in 0.1 M Tris-HCl pH 7.1, and set up for 4°C crystal trials using

various percentages of 2.0 M ammonium phosphate in 0.1 M Tris-HCl, pH 7.1. The amount of protein in some cases was limited, however if any stock protein remained, it was screened at 4°C using Hampton Crystal Screen I (Hampton Research) (Jancariak & Kim, 1991). Despite the increased purity of the protein samples crystals failed to grow in all cases.

## 2.5 Discussion

Despite successful crystallization from mixtures of some type III AFPs (Xue *et al.*, 1994), the isolation of AFPs from ocean pout sera presented several drawbacks; the most obvious being the difficulty to isolate homogeneous individual AFPs. Also, seasonal AFP variations in ocean pout (Fletcher *et al.*, 1984) resulted in compositional heterogeneity between different batches of G75 type III AFP. This did not simplify the task of reproducibly generating pure protein for crystal growth. Both of these concerns were further overshadowed by Dr. Fletcher's limited source of protein and the challenge of catching the fish and maintaining them at a natural temperature and photoperiod in aquaria until the sera was isolated (Fletcher, 1977). As for the most recent crystallization attempts, a lack of final product limited the range of crystal trials and thus reduced the chances of obtaining diffraction quality crystals. An unlimited homogeneous supply of easily-purified type III AFP would address all of the above concerns.

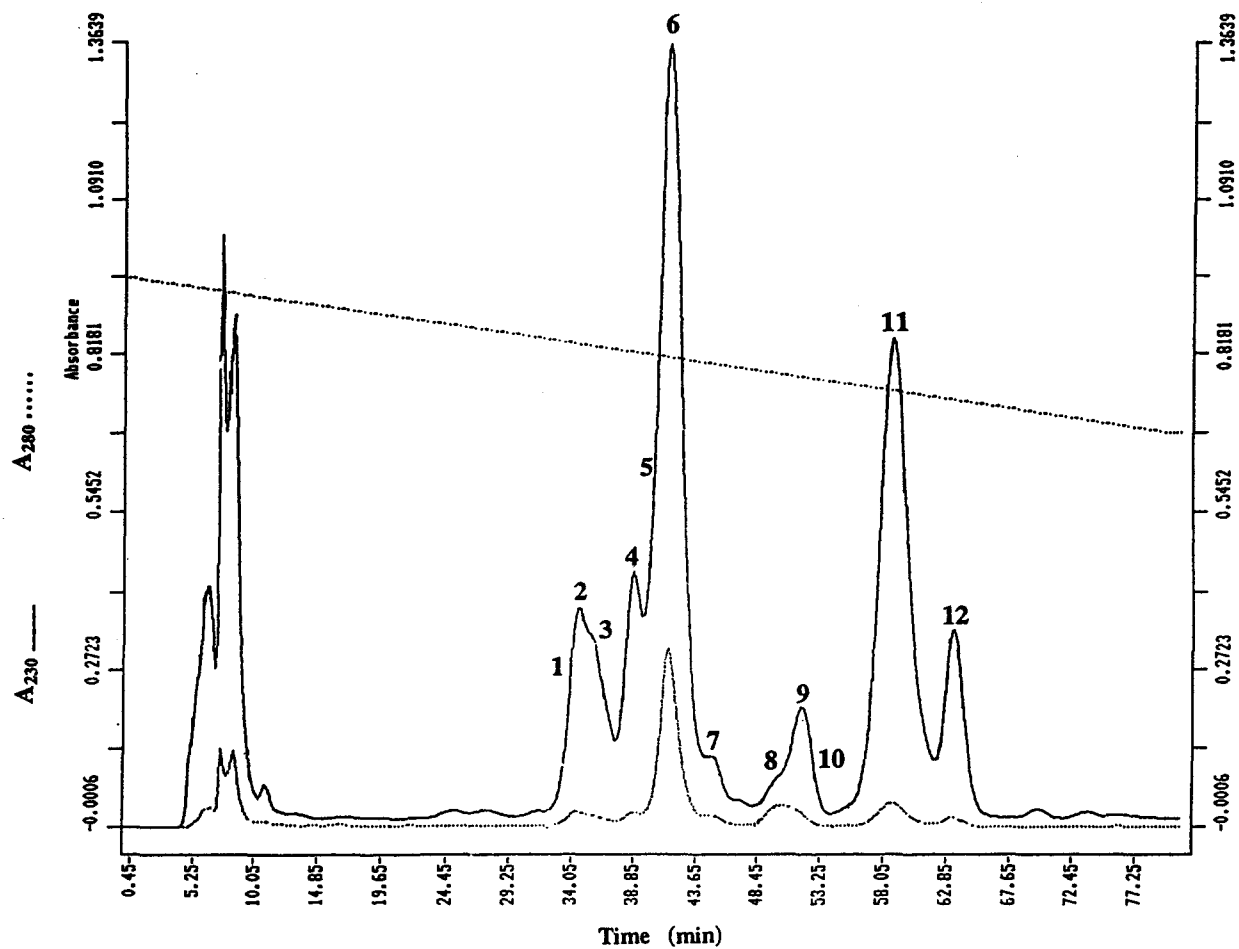


**Figure 2.1: Reverse phase purification of G75 type III AFP.** The twelve type III AFPs are shown as they elute from a Waters  $\mu$ Bondapak C18 column (7.8mm x 30cm) using 0.1% trifluoroacetic acid and a 1 ml/min gradient of 30% to 50% acetonitrile over 80 min.

HPLC	1	SQ	SVVATQLIPMNTALTPVMMEGKVTNPIGIPFAE	MSQIVGKQVNTPVAKGQTIMPNMVKTYAA
HPLC	4	-	-----I-----A-----	-----L-----V-G
HPLC	6	-	-----I-----A-----	-----L-----V-G
HPLC	7	-	-----R-----A-----	-----RI-----L-----
HPLC	9	-	-----A-----	-----RI-----L-----
HPLC	11	-	-----I-----A-----	-----RI-----L-----
cdNA	c10	-	-----S-----	-----M-----R-----K
cdNA	c7	-	-----I-----	-----L-----
genomic	λ5	-	-----I-----	-----L-----
wolffish	1.5	-	-----I-----I--K-Q-V--A-----	-----RA--DE-L-----R-A
wolffish	1.9	-	-----I-----I--K-Q-V--A-----	-----R--DE-L-----R-A
HPLC	12	N-A	---N---I---L---RSE-VT-V---	---DIPRL-SM---RA-PL-T-L--D---G-PPA
genomic	λ3	N-	---I---L---TTR-IY-T---	---DIPRL-SM---QA-PM-T-L--D---F-CLCAPLN
L.P.		NKA	---N---I---L---RAE-VT-A---	---DIPRL--L---RA-LI-T-L--D---G-PQ
R.D.		NKA	---N---I---LI--KAE-VT-M---	---DIPR-I-M---RA-PL-T-L--D---N-E
AB1		TK	---S---I---A--KA-EVS-K---	---E--K--M---RA-NDLE-L--D---T-Q
AB2		TK	---N---I---L---KAEVS-K---	---EIPRL--M---RA-YLDE-L--D---N-E

**Figure 2.2: Sequence homology exhibited by type III AFPs.** Conserved residues are replaced by dashes. The HPLC 1, 4, 6, 7, 9, 11, 12, c10, c7, λ3, and λ5 sequences are from ocean pout, *Macrozoarces americanus*. The remaining sequences are from other eel pouts: 1.5 and 1.9 are wolffish genomic clones; *Lycodes polaris* (L.P.); *Rhigophila dearborni* (R.D.); *Austrolycichthys brachycephalus* (A.B.). Reproduced from Davies & Hew, 1990.

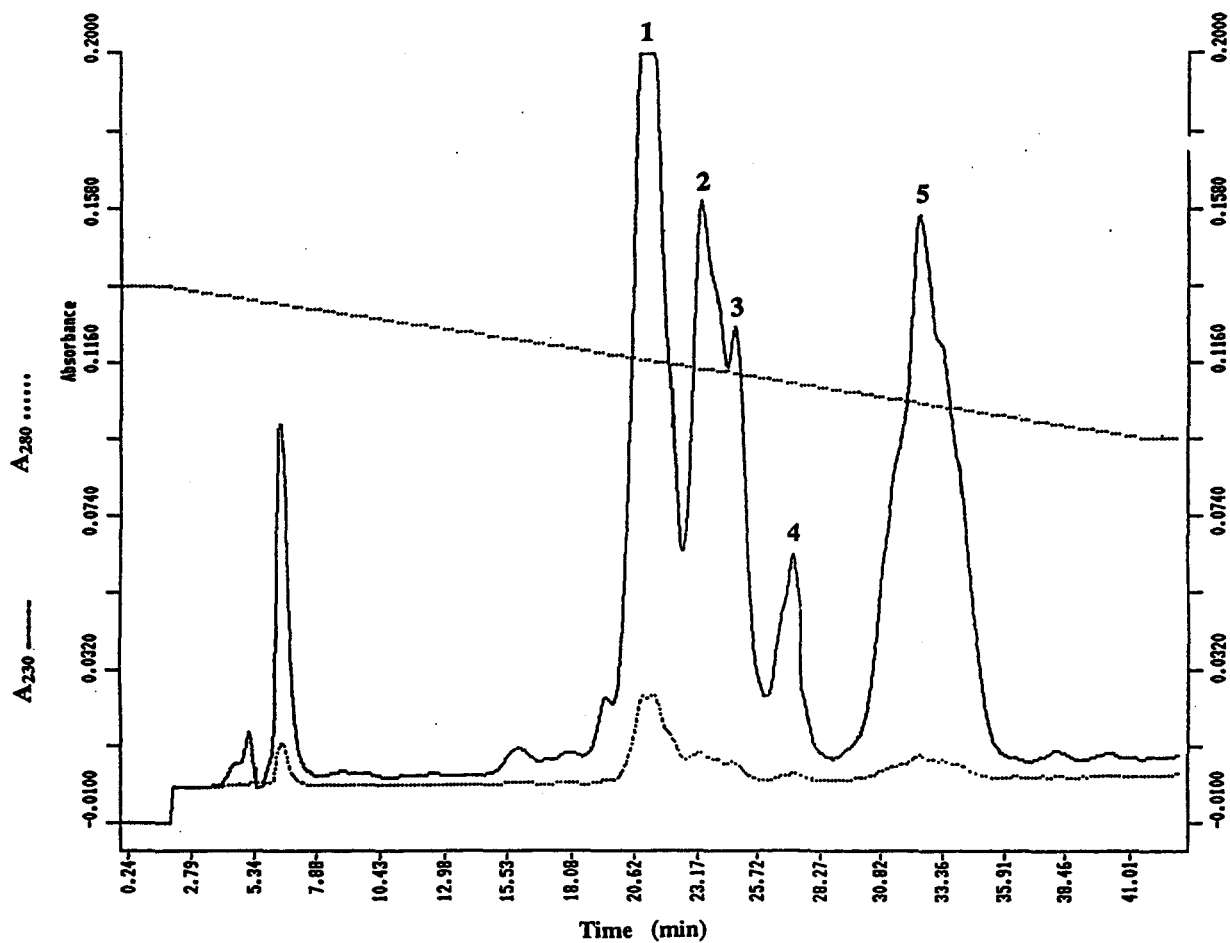
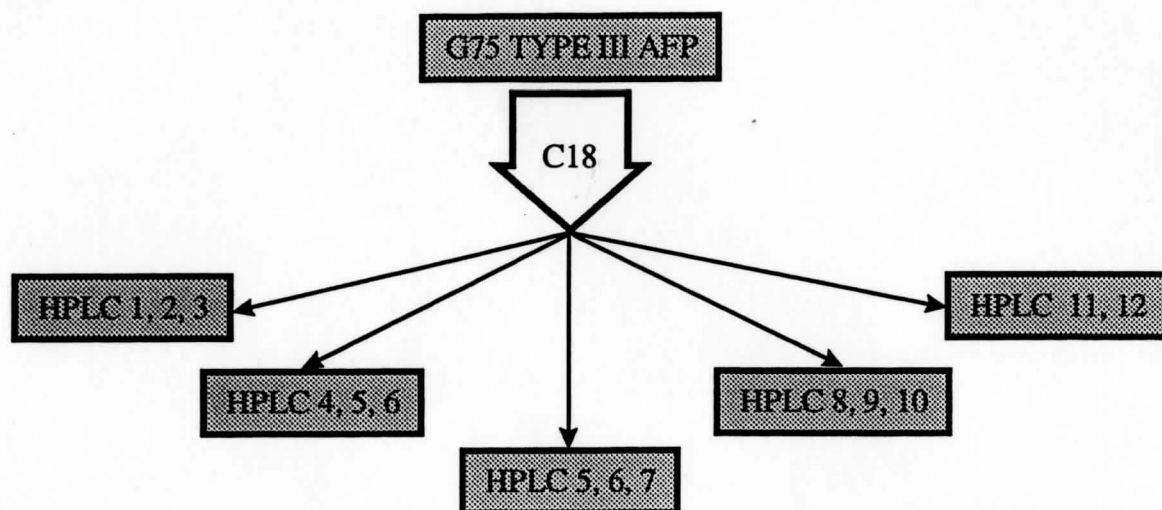


**Figure 2.3:** Elution profile from Xue *et al.*, 1994. G75 type III AFP was resolved into five peaks using a Waters  $\mu$ Bondapak C18 column (7.8mm x 30cm) with 0.1% trifluoroacetic acid and a 1ml/min gradient of 30% to 50% acetonitrile over 40 min.



**SYMBOLS:**

Co-eluted AFP isoforms

Column

Individual AFP

**Figure 2.4: Schematic of G75 type III AFP reverse phase purification.** The five peaks isolated by Xue *et al.*, 1994 are illustrated above from left to right. For example, peak 1 contained the HPLC 1, 2, and 3 isoforms.

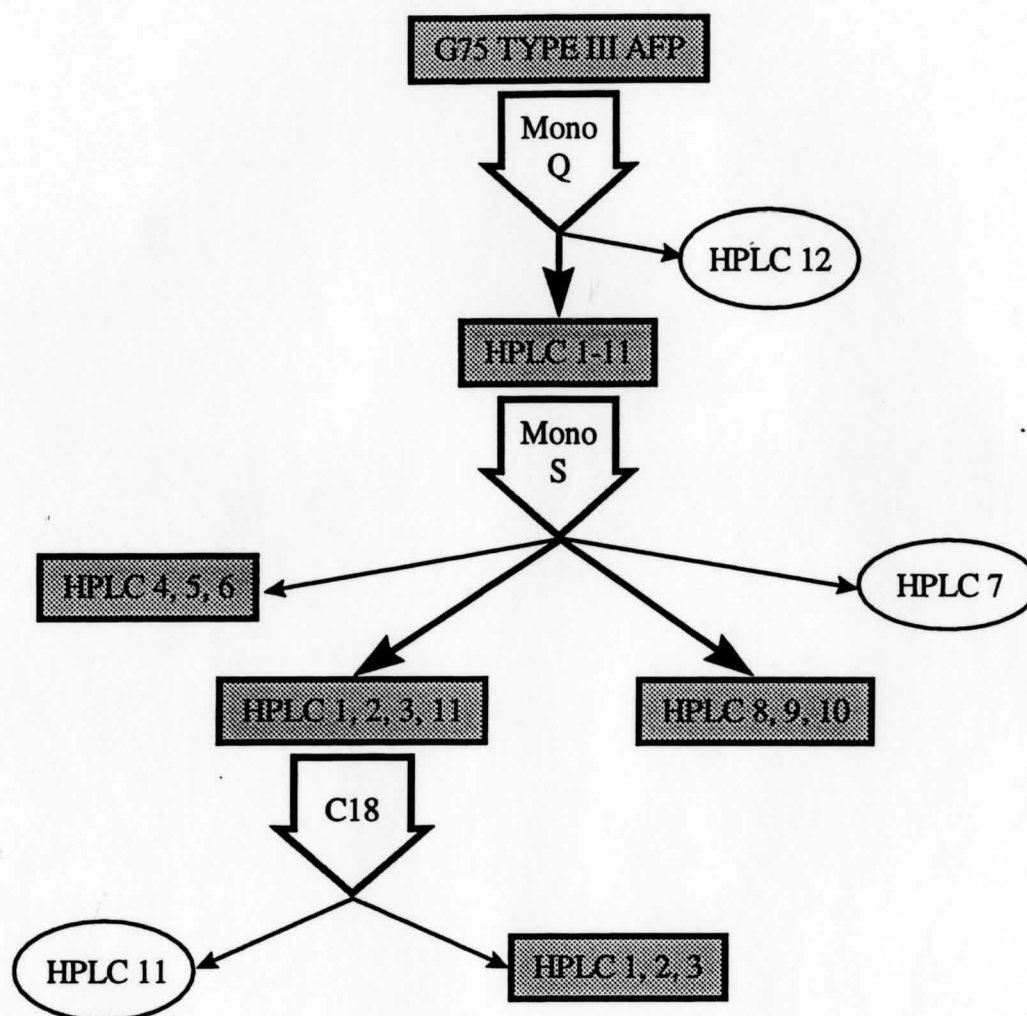


**Figure 2.5: Schematic of G75 type III AFP multiple-column purification.** A Mono-Q anion exchange column (Pharmacia, Montreal, QU) and a Mono-S cation exchange column (Pharmacia) were used to exploit different ion exchange binding affinities of the type III AFPs as in Li *et al.*, 1985. The C18 reverse phase purification followed the same procedure outlined in Figure 2.1.

## **CHAPTER THREE:**

---

# **OCEAN POUT HPLC 6 AFP FROM *E. COLI***

---

### **3.1 Introduction**

A second method for generating the large quantities of protein required for crystallography studies is via the use of a bacterial expression system. In order to assemble such a system, the gene corresponding to the protein of interest must first be identified and cloned from the organism in question. The full length cDNA clone for the HPLC6 type III AFP has been isolated and sequenced from an ocean pout cDNA library (Hew *et al.*, 1988). It codes for an 87 residue preprotein whose amino acid sequence is shown in Figure 3.1a. In 1991, Li *et al.* cleaved the original full length HPLC6 cDNA with *Hinf*I, and subcloned the 3' fragment into the  $\lambda$ PCIIL expression vector (from Song *et al.*, 1988). Recombinant HPLC6 AFP (rHPLC6) expressed from the resulting  $\lambda$ PCLII-rHPLC6 plasmid, lacked the 22 amino acid N-terminal presequence normally found on native HPLC6 AFP (Li, Trinh & Hew, 1991). Amino acid analysis confirmed the expressed rHPLC6 to be identical with the native mature HPLC6 from ocean pout, except for three additional residues: an N-terminal methionine as the start codon; a lysine

resulting from cDNA modifications; and a C-terminal lysine which was normally removed post-translationally in the native AFP (Figure 3.1: b, c). The additional residues (MK-HPLC6-K) were found to confer increased activity and thermal stability to the rHPLC6 AFP (Li, Trinh & Hew, 1991).

## **3.2 Purification of rmHPLC6 Using the pET His-tag<sup>®</sup> System**

### **3.2.1 Construction of the pET15b-rHPLC 6 vector**

The  $\lambda$ PCLII-rHPLC6 vector was generously provided by Dr. Choy Hew. In hopes of increasing expression efficiency via the *T7lac* promoter, and simplifying the purification through use of an N-terminal histidine tag, the rHPLC6 gene was removed from the  $\lambda$ PCLII-rHPLC6 vector via *NdeI* digestion, and inserted into the *NdeI* site of the pET15b vector (Novagen, Madison, WI). The pET15b-rHPLC6 product vector was digested with *PstI* to confirm the direction of the insert. The procedure is outlined in Figure 3.2. Unless otherwise noted, all molecular biology reagents/procedures were prepared/performed as outlined in *Current Protocols in Molecular Biology* (Ausubel *et al.*, 1993). Restriction digests, dephosphorylations, and ligations were performed according to the *New England Biolabs 1993/94 Catalog* and the individual NEB product guides. DNA fragments and vectors were purified from agarose gels using QIAEX beads (QIAGEN, Chatsworth, CA). The ligation mixture from Figure 3.2 (Step 3) was used to transform library efficiency DH5 $\alpha$ <sup>™</sup> competent cells (Gibco-BRL, Burlington, ON) by following their enclosed transformation protocol. DNA sequencing performed at the MOBIX Institute for Molecular Biology and Biotechnology (McMaster University, ON) confirmed the mutation-free generation of the product vector, pET15b-rHPLC6.

### 3.2.2 Expression of His-rHPLC 6 type III AFP

Competent *E. coli* BL21 (DE3) cells were prepared and transformed (Ausubel *et al.*, 1993) with gel-purified pET15b-rHPLC6 vector. Transformants were grown to saturation (37°C for 16 hours) in 5 ml and then 500 ml of LB-amp (0.5 µg/ml ampicillin). A 500 ml saturated culture was used to inoculate 25 L of LB-amp in a large scale fermentor (New Brunswick Scientific, Edison, NJ). Optimal growth occurred under the following conditions: 37°C; 30 psi air pressure; 18-20 L/min air flow; agitation of 150 rpm. Once the cell density reached an OD<sub>600</sub> of 0.8, expression of His-rHPLC6 AFP was induced using a final concentration of 0.5 mM isopropyl-β-D-thiogalactopyranoside. Optimal induction time was determined to be 3 hours, at which point the cells were harvested using a CEPA<sup>®</sup> continuous flow centrifuge (New Brunswick Scientific). The ~75 g cell pellet was resuspended in 300 ml of cold lysis buffer (20 mM Tris-HCl pH 7.9, 500 mM NaCl, 1 mM benzamidine, 1 mM phenylmethylsulfonyl fluoride), divided into six aliquots, and stored at -20°C.

### 3.2.3 Purification procedure (summarized in Figure 3.3)

Each 50 ml aliquot of cells was purified separately so as not to exceed the binding capacity of the nickel column. Cells were thawed and lysed at 4°C with a Fischer Model 300 sonicator (Fischer Scientific, Unionville, ON). Using the large probe, ten 15 second bursts at full power ensured complete lysis. The supernatant was isolated following centrifugation at 4°C and 20,000 x g for 20 minutes, and the successful expression of His-rHPLC6 was confirmed by the presence of ice-binding activity. The activity assay will be explained in detail in Section 3.3.

The supernatant was passed through a 30 ml DE52 column (Whatman, Clifton, NJ) pre-equilibrated at 4°C with lysis buffer. Active fractions collected from an isocratic elution were pooled, heated to 60°C while shaking, cooled to 10°C, and centrifuged at 20,000 x g for 40 minutes. With only heat-stable proteins remaining in the supernatant and all proteases inhibited and/or removed, the following purification steps were performed at room temperature without any degradation of the final rmHPLC6 product.

A 25 ml open column of His-bind<sup>®</sup> resin (Novagen) was prepared and charged with Ni<sup>2+</sup> using the following solutions: 60 ml H<sub>2</sub>O; 100 ml of 50 mM NiSO<sub>4</sub>; 60 ml of lysis buffer (without protease inhibitors). Once the post-heating supernatant was passed through the nickel column, any nonspecifically-bound proteins lacking the His-tag were removed with 250 ml of wash buffer (60 mM imidazole, 500 mM NaCl, 20 mM Tris-HCl pH 7.9). The His-rHPLC6 product was removed from the nickel column using 100 ml of elution buffer (1M imidazole, 500 mM NaCl, 20 mM Tris-HCl pH 7.9). The His-rHPLC6 eluted in a broad 50 ml peak, therefore, in preparation for thrombin cleavage, the eluate was concentrated to 5 ml in an Amicon cell (Amicon, Oakville, ON) using a YM3 membrane (3000 Da cutoff). Rather than dialysing the His-rHPLC6 in thrombin cleavage buffer (20 mM Tris-HCl pH 8.4, 150 mM NaCl, 2.5 mM CaCl<sub>2</sub>-added immediately prior to use), five serial 10:1 dilutions were performed in the Amicon cell to achieve the same result with minimal loss of protein. Thrombin cleavage was performed at room temperature overnight in a 5 ml volume with 200 units of thrombin. Cleavage at the thrombin site in the His-rHPLC6 AFP produced the His-tag and rmHPLC6 as products. The “m” in rmHPLC6 was added to distinguish the thrombin cleavage product AFP from rHPLC6 because thrombin cleavage left three additional amino acids on the N-terminal of rHPLC6 producing GSHMK-HPLC6-K. The amino acid sequences before and after

thrombin cleavage are illustrated in Figure 3.1. The cleavage reaction was then filtered with a 0.22  $\mu\text{m}$  syringe and purified via reverse phase HPLC to separate any uncleaved His-rHPLC6 from the His-tag and rmHPLC6 products (Figure 3.4).

In order to eliminate the need for serial dilutions of the nickel column eluate into thrombin cleavage buffer, the cleavage reaction was subsequently performed while His-rHPLC6 AFP remained bound to the nickel column. Therefore instead of using elution buffer, the nickel column was equilibrated with 200 ml of thrombin cleavage buffer immediately after the wash buffer step. Column flow was stopped when less than 1 ml of buffer remained above the resin bed, and 200 units of thrombin were added into this buffer. The resin was completely mixed with thrombin by repeated inversion of the column, and cleavage was allowed to proceed overnight at room temperature. Next, 50 ml of thrombin cleavage buffer was added to the column in 2 ml aliquots so as not to disturb the settled resin while eluting undiluted rmHPLC6. In this case, most of the His-tag and any uncleaved His-HPLC6 AFP remained bound to the nickel column. The eluate was concentrated to 5 ml in an Amicon cell (YM3 membrane), filtered to 0.22  $\mu\text{m}$ , and passed through a Waters C18 DeltaPak semi-preparative reverse phase column (19 mm x 30 cm). A 10 ml/min gradient using 0.1% trifluoroacetic acid with 30% to 40% acetonitrile over 40 minutes was sufficient for this separation. The collected rmHPLC6 peak was then lyophilized and stored at  $-20^{\circ}\text{C}$  for crystal trials. The final yield was ~350 mg of pure rmHPLC6 per 25 L fermentor culture. The amount of antifreeze protein remaining after each purification step is summarized in Table 3.1. A small amount of the rmHPLC6 peak was run through the (7.8 mm x 30 cm) Waters  $\mu$ Bondapak C18 analytical column (Figure 3.5) in order to offer a comparison with the G75 type III AFP profile from Figure 2.1.

### 3.3 Thermal Hysteresis Activity Assay

Due to its integral role throughout the purification process, the antifreeze activity assay will be explained at this time. Dilute antifreeze solutions (below 1 mM) can alter the morphology of a growing ice crystal (Knight, DeVries & Oolman, 1984), therefore melting and freezing temperatures can be directly determined by the visual observation of a growing ice crystal via light microscopy (Chakrabarty, Yang & Hew, 1989). A nanolitre osmometer (Clifton Technical Physics, Hartford, NY) was used to manipulate the temperature of a thermoelectrically-controlled microscope stage. A silver 7 x 7 x 0.35 mm sample holder was placed onto this microscope stage with a layer of zinc oxide paste in between to maximize contact and thermal transfer. Six holes (0.35 mm diameter) in the sample holder served as sample wells for the assay. Antifreeze solutions (10-20 nl) placed in any of the six wells were frozen within seconds by lowering the temperature to  $-40^{\circ}\text{C}$ . Once frozen, the wells were warmed until only a single ice crystal remained ( $\sim 50\ \mu\text{m}$  diameter). The melting temperature was defined as the point at which this single ice crystal melted at a constant rate, indicated by a decrease in diameter (Figure 3.6).

Subsequent cooling created freezing conditions which resulted in ice crystal growth. In the absence of AFPs, the ice crystal grew perpendicular to the *c* axis producing disks of larger diameter (Figures 1.2 and 3.6). However, the adsorption of AFPs to the pyramidal planes of ice (Knight, Driggers & DeVries, 1993), slowed ice growth parallel to the *a* axes causing concentration-dependent changes in ice crystal morphology. Dilute AFP solutions produced thin hexagonal plates while increasing AFP concentrations subsequently generated incomplete hexagonal bipyramids, complete bipyramids (Figure 3.6d), and finally needles (Yang, 1993). Regardless of the morphology, the freezing temperature was defined as the point where ice growth was no

longer suppressed. With bipyramidal and needle-shaped ice crystals, the freezing point was more obvious as indicated by a sharp spike of rapid freezing along the *c* axis (Figure 3.6e). The difference between freezing and melting temperatures in °C represented the amount of antifreeze activity. Each thermal hysteresis measurement was performed in triplicate with a maximum deviation of +/- 0.04°C.

### 3.4 Discussion

Initial difficulties encountered while attempting to purify individual type III AFP isoforms from the serum-derived G75 fraction (Chapter Two), justified an attempt to generate a bacterial expression system for one of the type III AFP isoforms. Since *E. coli* do not possess any endogenous proteins resembling type III AFPs, the expression of a single AFP isoform in *E. coli* eliminated the co-elution problems associated with resolving the nearly identical serum AFPs.

rHPLC6 type III AFP has been previously expressed and purified from *E. coli* (Li, Trinh & Hew, 1988). In this system, rHPLC6 was expressed under control of the heat-inducible  $\lambda$ pL promoter and purified using ammonium sulfate precipitation, Sephadex G75 resin, and reverse phase HPLC. The final yield of rHPLC6 was 0.5 mg per litre of bacterial culture. In order to increase expression levels using the T7lac promoter, and simplify large scale purification via an N-terminal histidine tag, the rHPLC6 gene was inserted into the pET15b expression system. When compared with bacterial growth in flasks, the use of a large scale 25 L fermentor promoted increased cell density due to a more thorough aeration of growing cultures. Also, the development of conditions facilitating efficient thrombin cleavage of His-rHPLC6 while bound to the nickel column,

significantly reduced the time required to purify a batch of protein. An entire 25 L fermentor could be processed in less than two weeks, generating 350 mg of pure rmHPLC6 type III AFP. Our yield of 14 mg/L of bacterial culture was a significant improvement relative to previous attempts with other expression systems.

The expression of His-rmHPLC6 was confirmed in the BL21 (DE3) cells by two methods. Using rabbit anti-G75 ocean pout antibodies provided by Dr. Choy Hew (Hew *et al.*, 1984), a single band of the correct size was detected on a Western blot. More convincing proof of His-rmHPLC6 expression was provided by the detection of antifreeze activity in the cell lysate; whereas lysates from both uninduced cells and cells with only the pET15b vector failed to produce any measurable antifreeze activity. This demonstration of antifreeze activity by His-rmHPLC6 was an extremely interesting result. His-rmHPLC6 (88 residues) was found to exhibit normal levels of antifreeze activity despite having an additional 22 amino acids added to the N-terminus of the original rHPLC6 AFP (68 residues) (Figures 3.7 & 3.8). This finding strongly suggested that the N-terminus of HPLC6 type III AFP is not involved in the ice binding mechanism.

Activity measurements were performed on a Clifton nanolitre osmometer as outlined in Section 3.3. Due to the small sample size, and the even smaller seed crystal size, flash freezing and supercooling were repeatedly uniform (Yang, 1993). In order to generate reproducible freezing and melting temperatures, care was taken to ensure the ice seed crystal was located in the middle of the sample well for each assay. Any contact with the sides of the well by the growing ice crystal would accelerate melting or freezing, depending on which process was occurring at the time. A second convention was implemented to account for the variable freezing temperatures caused by different rates of

cooling. Activity measurements were performed with AFP concentrations of 5 to 10 mg/ml to ensure the formation of complete bipyramidal ice crystals. Continued freezing would then produce the characteristic spike of ice growth parallel to the *c* axis (Figure 3.6e). Once spike growth was initiated, the sample well was warmed just to the point where further spike growth ceased. This value provided a reproducible freezing temperature regardless of the initial rate of cooling.

Thermal hysteresis values represent the noncolligative amount of freezing point depression afforded by AFPs. Since this activity is not affected by the concentration of other solutes present, the individual melting and freezing temperatures may vary in different buffers, however the range of activity remains unchanged (Yang, 1993). Therefore, the antifreeze activity of His-rHPLC6 and rmHPLC6 were exploited throughout the purification process. Activity values were used to quickly evaluate the presence of AFP at each step, and upon comparison with a standard curve (Figure 3.7) AFP concentrations were calculated (Table 3.1). This procedure was invaluable during initial refinement of the purification protocol so as to ensure maximum yields and continued activity after each purification step.

The establishment of a bacterial expression and purification system for rmHPLC6, has provided our laboratory with the unlimited homogeneous supply of protein required for crystal trials. A comparison of the reverse phase HPLC profiles for the serum-purified AFPs and the bacterial-derived rmHPLC6 (Figures 2.1 and 3.5 respectively) indicates the great improvement in purity provided by the latter case. This system will also prove valuable as the basis for future examination of type III AFP function via mutagenesis studies.



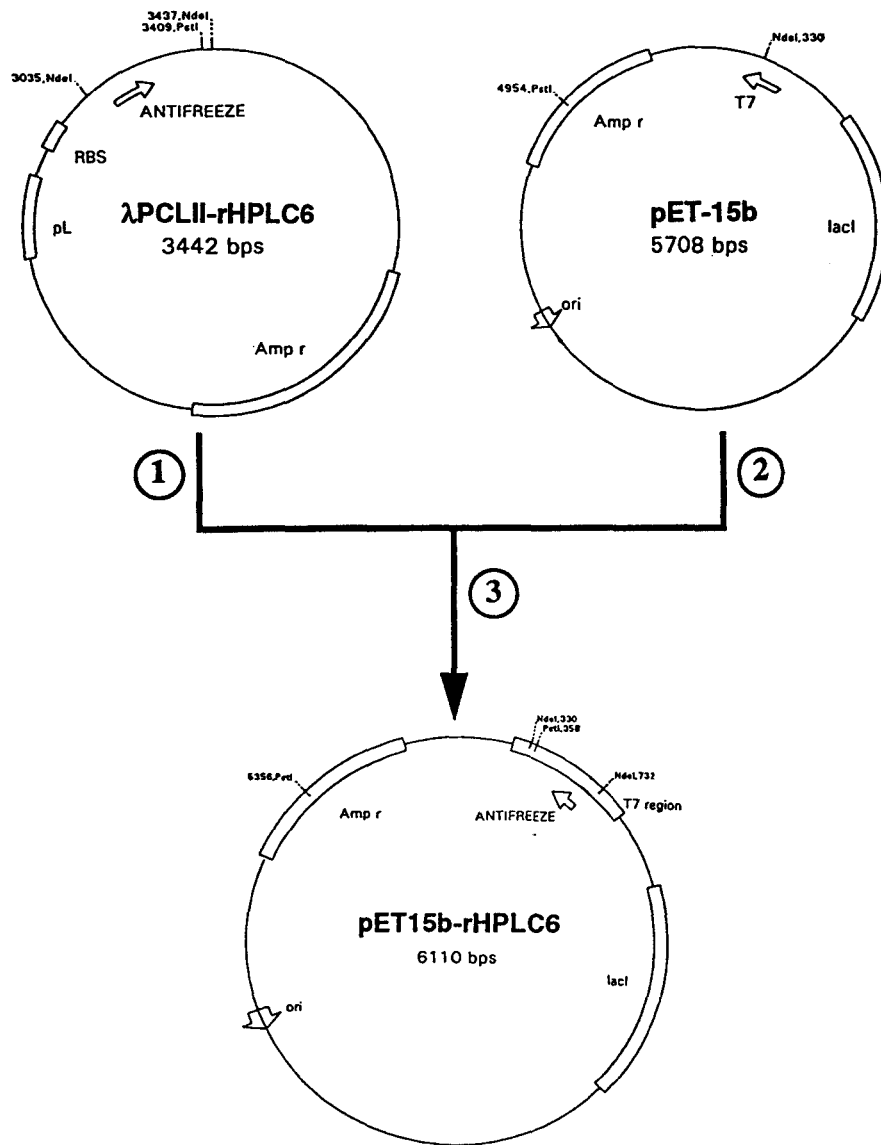


**Figure 3.2: Construction of the pET15b-rHPLC6 vector.** (1) The HPLC6 AFP gene was excised using *NdeI*\*, and gel purified. (2) The pET15b vector was linearized with *NdeI*\*, dephosphorylated using Calf Intestinal Alkaline Phosphatase\*, and gel purified. (3) The products of steps 1 and 2 were ligated using T4 DNA Ligase\* (1 hour at room temperature). Ligation product vectors were screened with a *PstI*\* digest to confirm insert direction. (\* New England Biolabs, Mississauga, ON)

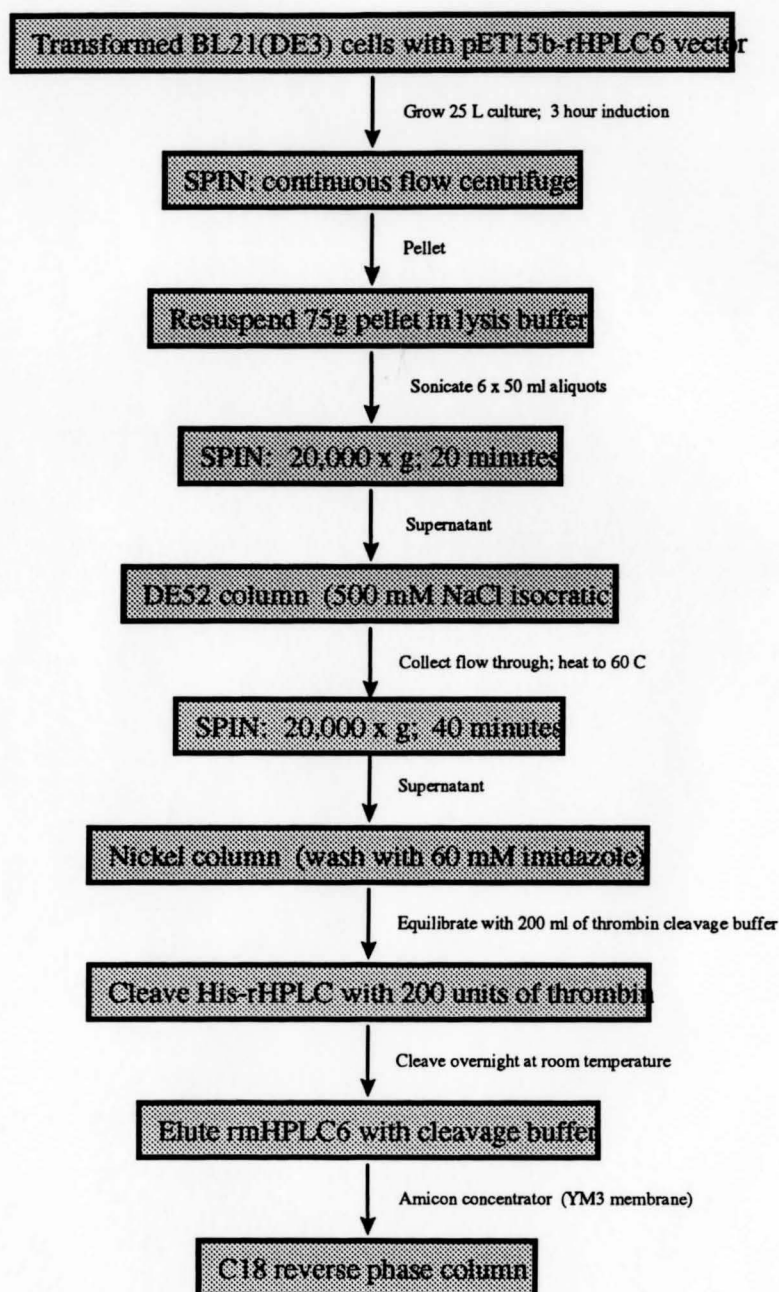


**Figure 3.3: rmHPLC6 purification summary.** The rmHPLC6 final product was collected off the C18 column and lyophilized. Total yield: 350 mg of pure rmHPLC6 from each 25 L fermentor culture.

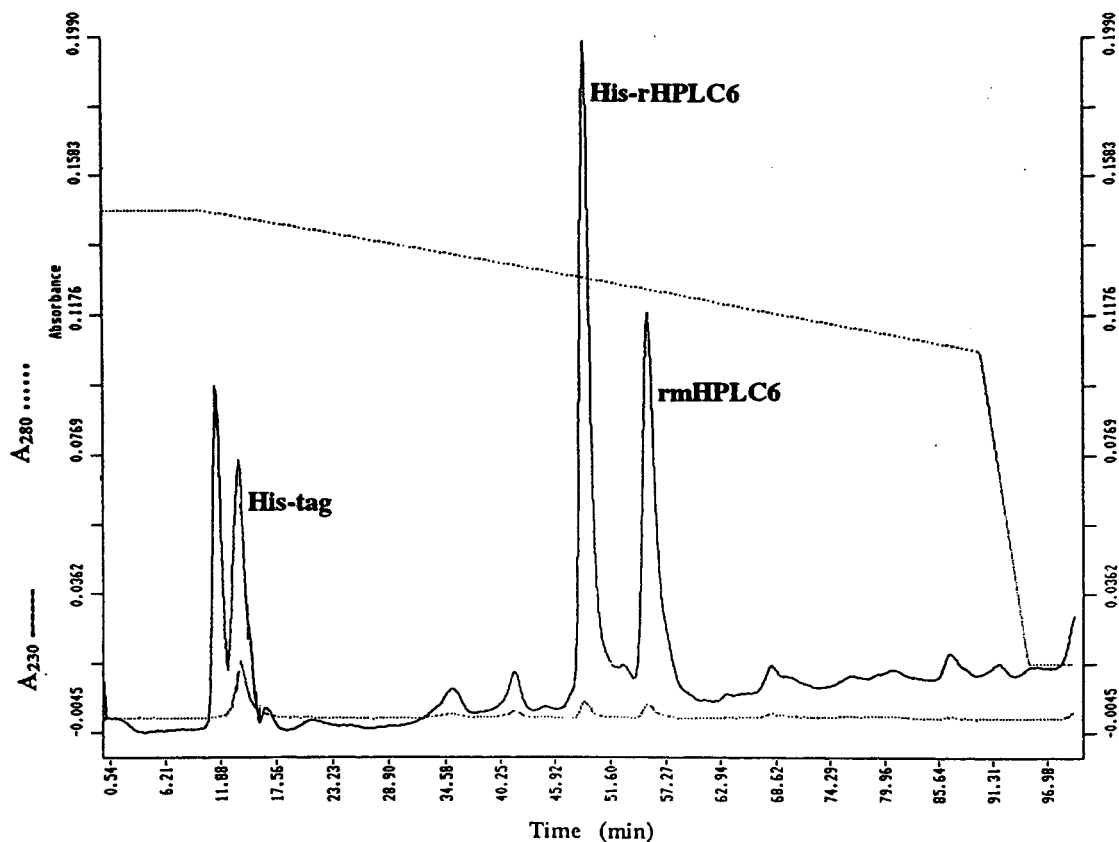


**Figure 3.4:** Reverse phase purification of the thrombin cleavage reaction products. The His-rHPLC6, His-tag, and rmHPLC6 cleavage products were separated by a Waters  $\mu$ Bondapak C18 column (7.8 mm x 30 cm) using 0.1% trifluoroacetic acid and a 1ml/min gradient of 25% to 45% acetonitrile over 80 minutes. The above cleavage reaction was approximately 25% complete.

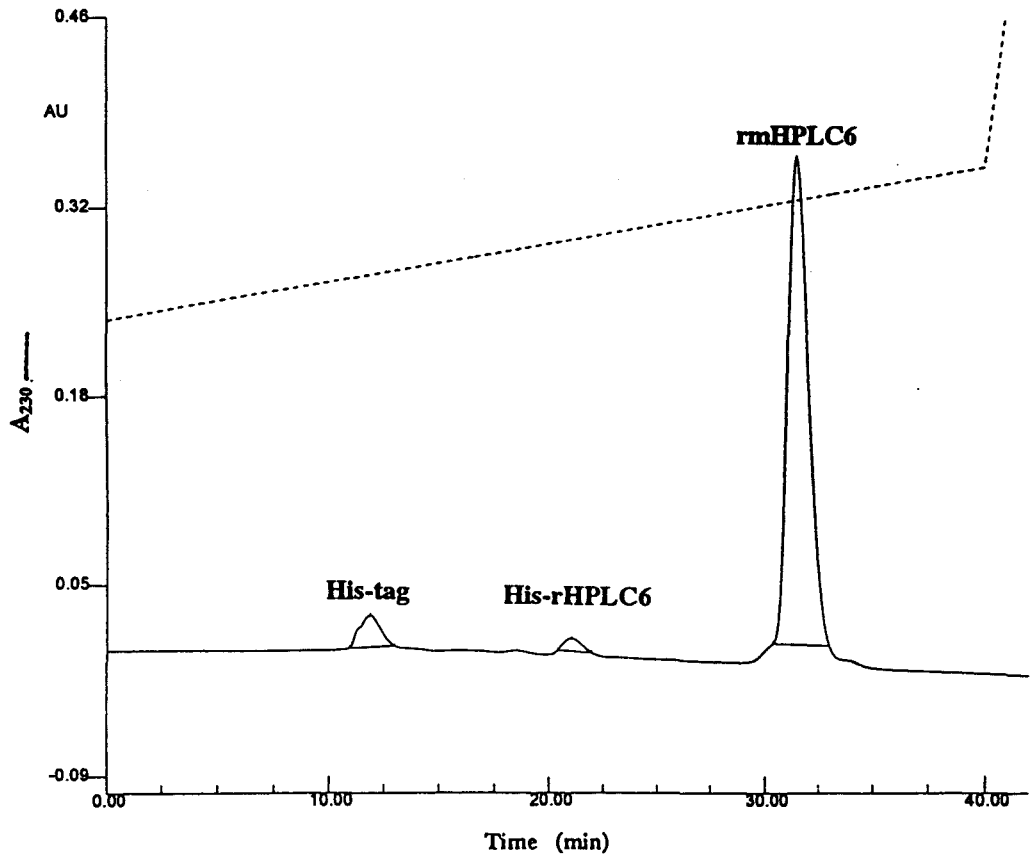
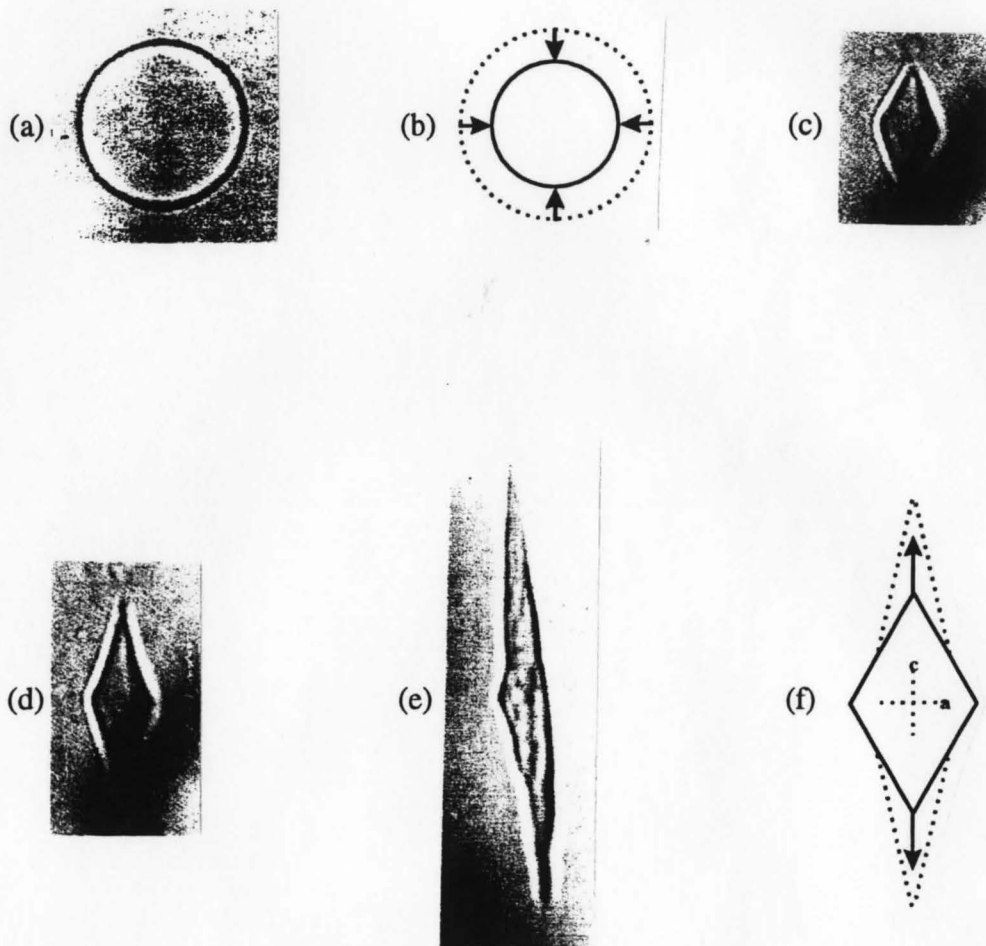


**Figure 3.5: Reverse phase profile of rmHPLC6 type III AFP.** Purification of the column-cleaved His-rHPLC6 eluate through a Waters  $\mu$ Bondapak C18 column (7.8 mm x 30 cm) using 0.1% trifluoroacetic acid and a 1 ml/min gradient of 25% to 35% acetonitrile over 40 minutes. The final purity of rmHPLC6 is significantly improved in comparison with the resolution of serum-purified HPLC6 (Figure 2.1).



•Antifreeze Activity ( $^{\circ}\text{C}$ ) = Freezing temperature - Melting temperature•

**Figure 3.6: Thermal hysteresis activity assay.** (a) A stable, 50  $\mu\text{m}$  single ice crystal in the center of a sample well (40X). (b) Warming induces the crystal to melt at a constant rate (the melting temperature). (c) Cooling induces expression of ice faces, resulting in a bipyramidal ice crystal (20X). (d) This shape is maintained despite further cooling until (e) a rapid spike of uninhibited growth occurs parallel to the  $c$  axis (20X). (f) Warming of the spiked-bipyramid crystal will stop further spike growth (the freezing temperature).

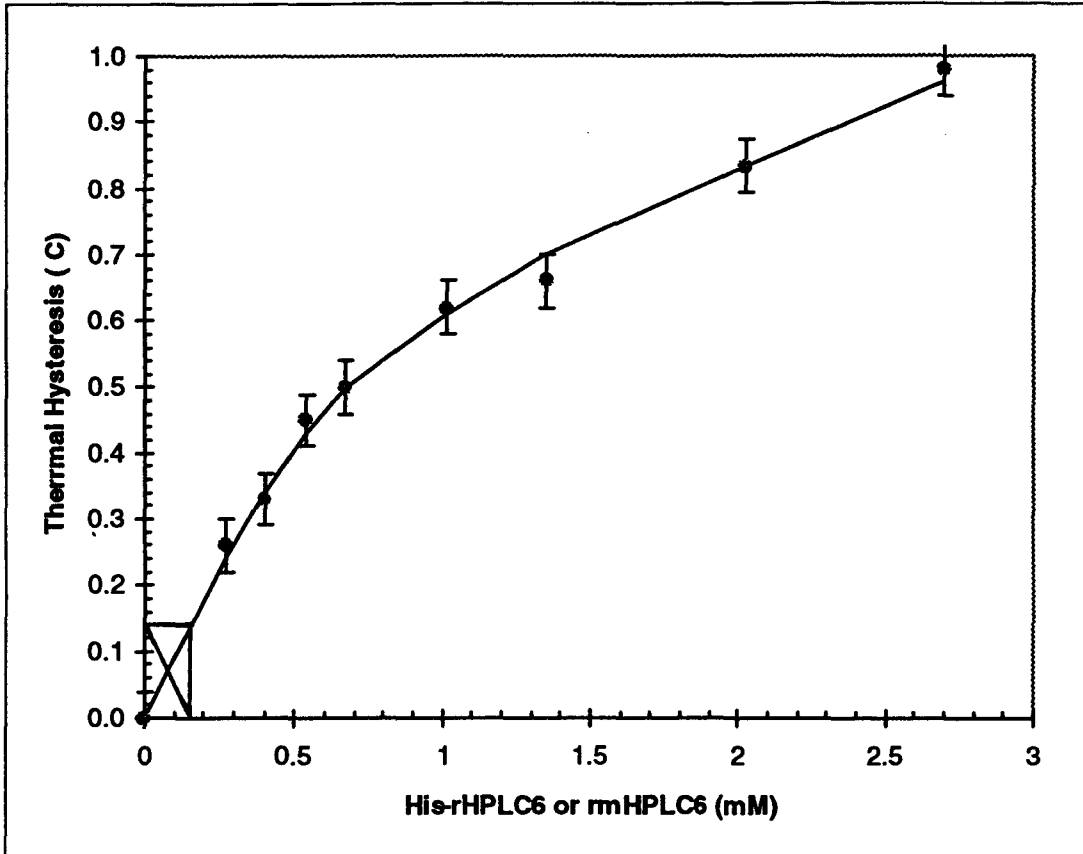


**Figure 3.7: rmHPLC6 standard curve.** Protein concentration was determined using the BCA Protein assay (Pierce). Thermal hysteresis values were derived using a Clifton nanolitre osmometer (Clifton Technical Physics). Each thermal hysteresis measurement was performed in triplicate with a maximum deviation of  $\pm 0.04^{\circ}\text{C}$ . Activities below  $0.14^{\circ}\text{C}$  were difficult to measure and were not used. A comparison of this curve with the ocean pout hysteresis curves (Figure 3.8) indicates that the recombinant His-rHPLC6 and rmHPLC6 AFPs exhibit normal activity levels.

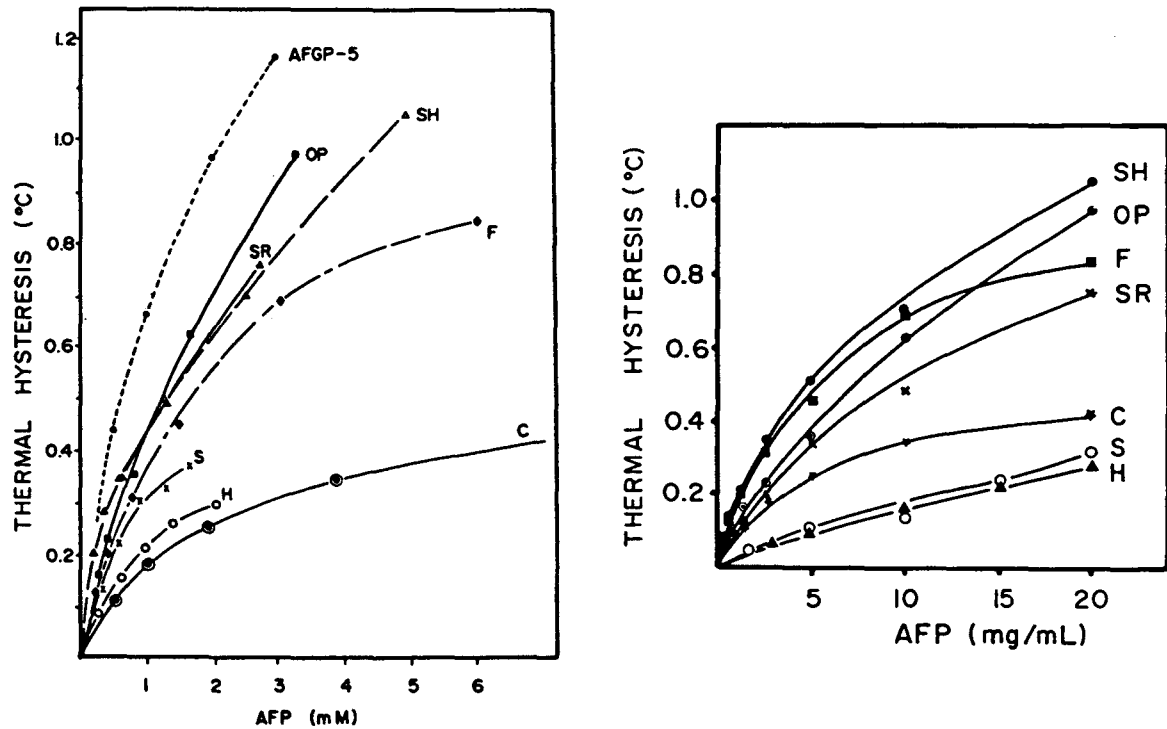


**Figure 3.8:** A comparison of thermal hysteresis curves for fish AFPs and AFGPs. Measurements were made on a Clifton nanolitre osmometer using AFPs and AFGPs isolated from the following fish: shorthorn sculpin (SH); ocean pout (OP); winter flounder (F); sea raven (SR); Atlantic cod (C); smelt (S); and Atlantic herring (H). Reproduced from Ewart & Fletcher, 1990.

**Table 3.1: Purification table for rmHPLC6.**

(refer to Figure 3.3 for the purification scheme)

Purification Step	Volume (ml)	Activity (°C)	[AFP] (mM)	His-rHPLC6 (mg)	rmHPLC6 (mg)
Cell lysate	50	0.45	0.54	236	
SPIN					
Supernatant 1	48	0.45	0.54	228	
DE52 FT	60	0.30	0.35	185	
HEAT & SPIN					
Supernatant 2	55	0.33	0.38	182	
Nickel column FT	55	< 0.14	< 0.15	16*	
Nickel column wash	250	< 0.14	< 0.15	67*	
TCB equilibration	200	0	0	0	
Post-cleavage eluate	50	0.24	0.26		96
Amicon FT	45	< 0.14	< 0.15		25*
Amicon retentate	5	0.82	1.89		70
C18 rmHPLC6 peak	100**				
Post lyophilization					59

\* Dilute samples resulted in activity values below 0.14°C, thus exact protein concentrations could not be determined for these solutions. In each case (Nickel column flow through, Nickel column wash, Amicon flow through) the presence of any antifreeze activity represented a loss of protein. The BCA assay (Pierce) was used to check the concentration of these samples.

\*\* Since the acetonitrile/water eluate from the reverse phase column would not freeze, activity measurements could not be performed.

## **CHAPTER FOUR:**

---

# **rmHPLC6 CRYSTALS, DERIVATIVES AND DATA COLLECTION**

---

### **4.1 Crystallization of rmHPLC6 Type III AFP**

Lyophilized rmHPLC6 was resuspended in 0.1 M Tris-HCl pH 7.1 to a concentration of 40 mg/ml, as determined by the BCA protein assay (Pierce, Rockford, IL). Initial crystallization conditions were obtained with a sparse matrix screening method (Jankariak & Kim, 1991) using Hampton Crystal Screens I & II (Hampton Research). The 98 crystallization conditions were tested each at room temperature and 4°C via the hanging drop vapour diffusion method (Wycoff *et al.*, 1985). 4µl and 12µl drops were formed for each of these screens using 1:3, 1:1, and 3:1 ratios of protein solution to crystal screen respectively. The drops were then vapour sealed to equilibrate with a reservoir of 0.7 ml of the respective crystal screen. The only condition which reproducibly yielded tiny crystals was Hampton Screen #2.48: 0.2 M ammonium phosphate, 0.1 M Tris-HCl pH 8.5, and 50% v/v MPD (2-methyl-2,4-pentanediol). While at 4°C, crystal clusters appeared overnight and reached maximum size in a few days (Figure 4.1). The

concentrations of both MPD and protein were each decreased in an attempt to slow crystal growth and generate larger crystals, but little improvement was achieved. Wells were micro seeded (Stura & Wilson, 1992) with serum-derived Peak 1 and Peak 3 type III AFP micro-crystals (Xue *et al.*, 1994), however this method to generate larger crystals also proved unsuccessful.

As outlined in Table 2.1, the crystallization conditions which yielded diffraction quality crystals for Peak1 and Peak3 type III AFPs (Xue *et al.*, 1994) were attempted with rmHPLC6. Protein concentration, the proportion of crystallization solution in the drop, and pH were varied at room temperature and 4°C. Extremely large diffraction quality crystals of 1.2 x 0.57 x 0.15 mm (Figure 4.2) were generated at room temperature over three days in drops with 2 µl of 16 mg/ml rmHPLC6 (in 0.1 M Tris-HCl pH 7.1) and 2 µl of a variation of Hampton Crystal Screen 1.04: 0.068 M Tris-HCl pH 8.0 and 2.72 M ammonium sulfate. Initially, crystals were mounted in 0.7 mm diameter capillary tubes and data collection was performed at room temperature using the system described in Section 2.3. DENZO (Otwinowski, 1993) was used to determine the diffraction limit, space group, and unit cell dimensions: 2.1Å, C222<sub>1</sub>, a = 77.053Å, b = 109.651Å, c = 38.137Å with 2 rmHPLC6 molecules per asymmetric unit. All data collection statistics are summarized in Table 4.1.

## 4.2 Additional Cloning Experiments

As outlined in Section 2.2, serum-purified type III AFPs readily crystallized with two original Hampton Crystal Screen solutions. Therefore, the initial difficulties identifying crystallization conditions for rmHPLC6 from either of the Hampton Crystal

Screen Kits provided cause for concern. Six additional non-native amino acids in rmHPLC6, five on the N-terminus and a lysine on the C-terminus, were suspected to be interfering with the crystallization process (Figure 4.3c). To address this problem, PCR primers (Ausubel *et al.*, 1993) were designed to modify the N-terminal GSHMK into an enterokinase cleavage site and to also replace the C-terminal lysine with a stop codon (Figure 4.3d). The following PCR primers were synthesized by the MOBIX Institute for Molecular Biology and Biotechnology (McMaster University, ON):

5'-GGG AAT TCC ATA TGG ACG ACG ACG ACA AAC AAT CAG TAG TAG C-3'

5'-CGC GGA TCC CTA TCC CGC GAC GTA CGT-3'

The primers were also designed to generate *Bam*HI and *Nde*I ends to facilitate reinsertion into pET15b. The PCR product was gel-purified, cleaved with *Bam*HI and *Nde*I and ligated to a gel-purified pET15b vector linearized by *Bam*HI and *Nde*I digests (NEB Catalog and Product Guides, 1993). DNA sequencing by the MOBIX Institute for Molecular Biology and Biotechnology (McMaster University, ON) confirmed that no mutations occurred in the desired fragment during PCR amplification. Expression of His-eHPLC6 (Figure 4.3d) in *E. coli* BL21 (DE3) cells was confirmed by lysate antifreeze activity levels similar to those displayed by His-rHPLC6. Expressed His-eHPLC6 was purified by the same procedure outlined in Section 3.2, although enterokinase cleavage conditions have yet to be determined. Successful cleavage with enterokinase would generate native HPLC6 (Figure 4.3e) for crystallization and structural studies.

## 4.3 Preparation of Heavy Atom Derivatives

### 4.3.1 Crystal soaking

Uranyl nitrate, uranyl acetate, samarium nitrate, samarium acetate, trimethyllead acetate, and terbium nitrate were chosen as potential heavy atoms because each of these compounds show preferential binding to glutamate residues (Petsko, 1985; Holden & Rayment, 1991). Such interaction would provide each compound with two potential binding sites per rmHPLC6 molecule. In order to minimize crystal handling and the potential for damage, crystals were not moved into heavy atom solutions for soaking. Instead, appropriate amounts of saturated heavy atom stock solutions were added to the reservoir of each hanging drop chamber to generate 1 mM to 50 mM heavy atom soaking solutions. The original mother liquor comprising the hanging drop was carefully removed with a glass capillary tube, leaving the crystal sitting on the cover slip. Immediately, 10  $\mu$ l of the heavy atom solution from the crystallization well was then placed around the crystal to re-form the hanging drop. Soaks were performed in the dark to eliminate any potential photochemical reactions. With each compound listed above, both heavy atom concentration and length of soak were varied to generate isomorphous rmHPLC6 crystals with maximum heavy atom exposure, such that any increase in heavy atom concentration or length of soak would immediately crack the crystals (Figure 4.4). X-ray data was collected at room temperature from stable soaked rmHPLC6 crystals. In every case the merging of heavy atom x-ray data with native data produced an R-merge of 4-6%, indicating an absence of heavy atom incorporation in the rmHPLC6 crystals. Raw x-ray diffraction data was processed using DENZO and SCALEPACK (Otwinowski, 1993). Heavy atom data sets were scaled and merged with native data using the PHASES software package (Furey & Swaminathan, 1990).

Due to the lack of success with glutamate-targeting heavy atom compounds, iodination was attempted in hopes of exploiting the single tyrosine residue in rmHPLC6 AFP (Figure 4.6c). Based on previous experiments which successfully iodinated tyrosine residues in  $\alpha$ -chymotrypsin crystals (Sigler, 1970), a concentrated stock solution was prepared: 15 mM  $I_2$  in 0.15 mM KI. As previously detailed, the stock was diluted into the reservoir solution of a hanging drop chamber and then the dilution was used to re-form the hanging drop around a rmHPLC6 crystal on the cover slip.  $I_2$  and KI react to form  $I_3^-$  which iodates the phenyl ring of the tyrosine residue, however no iodine incorporation was observed in the soaked isomorphous rmHPLC6 crystals (Means & Feeney, 1971).

#### **4.3.2 Cross-linking with gluteraldehyde**

In order to permit longer soaks with higher heavy atom concentrations, crystal stability was increased via cross-linking with gluteraldehyde (Matthews, 1985). Crystals were incubated in a solution of 0.25% gluteraldehyde for three hours. Completion of the cross-linking reaction was indicated by the clear transparent crystals adopting a yellow colour. Room-temperature data collected on cross-linked rmHPLC6 crystals merged well with native data (R-merge of 4-6%) indicating the crystals were isomorphous. Treated crystals were stable indefinitely in a variety of different buffers, and were also resistant to increased concentrations of each previously-mentioned heavy atom compound. Some heavy atom compounds are known to induce protein crystals to change colour upon incorporation (Petsko, 1985). Soaks with iodine and uranyl acetate both generated stable bright red rmHPLC6 crystals, however in these and all other soaking trials on cross-linked crystals, x-ray data failed to indicate heavy atom incorporation.

### 4.3.3 Iodination of rmHPLC6 in solution

Since the task of diffusing heavy atom compounds into existing rmHPLC6 crystals was proving to be difficult, an attempt was made to derivatize the protein in solution and then crystallize the complex (Means & Feeney, 1971; Petsko, 1985). Pure 16 mg/ml rmHPLC6 in 0.1 M Tris-HCl pH 7.1 was iodinated in solution via a 2 hour incubation with a mixture of 0.075 mM I<sub>2</sub> and 0.150 mM KI (final concentrations). This solution was passed through a 0.22 µm syringe filter and the reaction mixture was resolved on a 7.8 mm x 30 cm Waters µBondapak C18 reverse phase column. Excellent separation into three distinct peaks was achieved using 1 ml/min 0.1% trifluoroacetic acid with a 33% to 36% acetonitrile gradient over 50 minutes (Figure 4.5). Each peak was collected, lyophilized and identified by electrospray mass spectral analysis (McMaster Regional Centre for Mass Spectrometry, McMaster University, ON). Mono-iodinated and di-iodinated products were confirmed to differ from rmHPLC6 by the mass of one and two iodine atoms respectively (Figure 4.6). An initial reaction using 30 mg rmHPLC6 yielded 10 mg of mono-iodinated product, and 2mg of di-iodinated product. Any unreacted rmHPLC6 was recovered and used in subsequent iodination reactions.

The mono-iodinated and di-iodinated rmHPLC6 products were resuspended in 0.1 M Tris-HCl pH 7.1 to a final concentration of 16 mg/ml and set up for hanging drop vapour diffusion crystal trials. Mono-iodinated rmHPLC6 crystallized under the same conditions as rmHPLC6 (Section 4.1), although seeding with rmHPLC6 micro-crystals was required to initiate crystal growth (Stura & Wilson, 1992). Hanging drops were composed of 2 µl of 16 mg/ml protein stock and 2 µl of the crystallization solution (0.068 M Tris-HCl pH 8.5; 2.72 M ammonium sulfate). Crystals grew at room temperature over

seven days (Figure 4.7). The di-iodinated rmHPLC6 precipitated under the same conditions.

#### 4.3.4 Selenomethionyl rmHPLC6

Another method used to incorporate heavy atoms into target protein is by expressing the protein in bacteria in the presence of a derivatized amino acid. Methionine auxotrophic B834TN60 *E. coli* cells were transformed with pET15b-HPLC6. Cells initially grown in LB-amp were isolated (20,000 x g for 15 minutes) and transferred to minimal media (Ausubel *et al.*, 1993) supplemented with seleno-L-methionine prior to induction according a slightly modified procedure of Graber *et al.*, 1993. A 4 L bacterial culture yielded 15 mg of pure Se-rmHPLC6, isolated according to the purification procedure outlined in Section 3.2. Mass spectral analysis (McMaster Regional Centre for Mass Spectrometry, McMaster University, ON) confirmed 100% incorporation of selenomethionine into Se-rmHPLC6. Lyophilized protein was resuspended to 16 mg/ml in 0.1 M Tris-HCl pH 7.1 and crystallized in a similar fashion as rmHPLC6 and I-rmHPLC6 using 0.068 M Tris-HCl pH 8.5 with 2.72 M ammonium sulfate. Crystals were irregular in shape and rather small (approx. 0.1 x 0.1 x 0.1 mm) in comparison with rmHPLC6 and I-rmHPLC6 crystals (Figure 4.8). Data collection was attempted on Se-rmHPLC6 crystals using the X12C Beamline at the National Synchrotron Light Source, Brookhaven, NY., however the few existing crystals were damaged during freezing. These highly mosaic crystals diffracted poorly, therefore collection of high quality x-ray data was not possible.

#### 4.4 Cryocrystallographic Data Collection

In order to collect x-ray data of the highest quality, cryocrystallographic techniques were used (Walter *et al.*, 1995). The acquisition of a cooling device from Molecular Structure Corp. allowed our laboratory to maintain a crystal temperature of -165°C for unlimited lengths of time during data collection. Initial efforts were focused on the identification of a suitable cryoprotective solvent and development of crystal soaking and freezing techniques. rmHPLC6 crystals were test-soaked in a variety of cryoprotectants such as 15 to 40% PEG 8000, 15 to 25% glycerol, immersion oil, and 30 to 60% v/v MPD. Crystals were determined to be most stable in immersion oil and also in a solution of 20% glycerol prepared with crystal mother liquor (0.068M Tris-HCl pH 8.0; 2.72 M ammonium sulfate).

In order to sufficiently bathe crystals in the chosen cryoprotectant, soaks of only a few seconds were required. To facilitate speedy crystal manipulation, crystals have traditionally been transferred into and out of cryoprotectants using tiny fiber loops of a diameter slightly larger than the crystal size (Walter *et al.*, 1995). Transfer in this fashion was problematic for rmHPLC and I-rmHPLC6 crystals due to their large size, often resulting in cracked crystals. Crystals were therefore drawn out of the original wells using a 0.7 mm diameter capillary tube and released into the cryoprotectant within a vesicle of mother liquor. The action of looping the crystal out of this solution drew the crystal out of its mother-liquor filled drop and through the cryoprotectant on its way out of the cryoprotectant/mother liquor emulsion.

Mounting loops were created by fastening a thin rayon loop to a metal mounting pin. Crystals were looped out of the cryoprotectant and flash-frozen via direct insertion

into the nitrogen stream. A magnetic base on the mounting pin secured the frozen crystal mount to a magnetic goniometer head. To slow frost accumulation on the crystal, a crude box was constructed out of thin plastic sheets to enclose the collimator, goniometer head, nitrogen stream and the detector surface. Data was collected at  $-165^{\circ}\text{C}$  on the serum-purified type III AFPs, rmHPLC6, and I-rmHPLC6 crystals using the system outlined in Section 2.2. In each case, DENZO and SCALEPACK (Otwinowski, 1993) were used with a 15 minute  $1.5^{\circ}$  oscillation frame to determine the diffraction limit, space group, and unit cell dimensions (summarized in Table 4.1).

## 4.5 Discussion

Diffraction quality rmHPLC6 crystals were generated using conditions similar to those earlier found to crystallize the serum-purified Peak1 and Peak3 AFPs (Section 2.2), with the only significant difference being an increase in ammonium sulfate concentration. The rmHPLC6 crystals attained maximum size ( $1.2 \times 0.57 \times 0.15$  mm) over only three days, in comparison with the Peak 1 and Peak 3 crystals which required seven weeks to reach a substantially smaller size. This increased rmHPLC6 crystal growth rate is perhaps a reflection of both the increased precipitant concentration and the absence of AFP microheterogeneity in the purified rmHPLC6 samples.

During an x-ray diffraction experiment, electrons along the repeating planes in a crystal lattice will diffract the incident x-ray beam. Diffracted beams are identified on an imaging plate, however only the intensity of the resulting spots can be accurately measured. In order to generate an electron density map and solve a macromolecular structure, the phase of each diffracted beam must be determined. One method to obtain

phasing information is by isomorphous replacement. This involves derivatizing the protein of interest with a particular heavy atom compound such that it adopts a very ordered position in the crystal lattice and alters the diffraction pattern. If the derivatized crystal remains isomorphous with native crystals, then any differences in diffracted intensities can be directly attributed to scattering from the electron-rich heavy atoms. From this information the heavy atom positions can be identified and used to subsequently determine the phases for each intensity measurement.

The most successful method of generating isomorphous heavy atom crystals has traditionally been via soaking native crystals in heavy atom solutions prepared with the crystal mother liquor (Petsko, 1985; Stura & Chen, 1992). By diffusion, the heavy atom compound distributes throughout the solvent channels in the crystal and then interacts with preferred binding sites. A minimal number of heavy atom binding sites are desirable on the target protein because a large number of incorporated heavy atoms makes their identification on a Patterson map increasingly difficult. Additionally, the crystal may suffer an alteration of its packing arrangement and thus become non-isomorphous. Platinum and gold complexes have often served as the more successful heavy atom compounds, binding to histidine above pH 6, methionine at any pH, and lysine above pH 9 (Petsko, 1985). However, the 71 residue rmHPLC6 (Figure 4.3c) contains 1 histidine, 6 methionine and 6 lysine residues thus eliminating use of both the platinum and gold complexes at any pH due to an overabundance of binding sites. Mercurial compounds, although another popular choice in isomorphous replacement experiments, could not be used due an absence of cysteine residues in rmHPLC6.

Lanthanides and uranyl salts interact with aspartate and glutamate residues above a pH of 5. Having only two glutamate residues in rmHPLC6, these compounds served as a reasonable starting point. As previously mentioned, soaked crystals were examined by x-ray analysis for heavy atom incorporation at various points during the soaking reactions, however even up to the point of crystal cracking, no bound heavy atoms were detected. A possible explanation for the lack of incorporation was the tendency of ammonium sulfate buffer to produce the  $\text{NH}_3$  nucleophile above pH 6. Therefore crystals were cross-linked with glutaraldehyde and soaked in various other buffers such as sodium citrate and lithium sulfate. Crystals remained isomorphous and displayed increased stability, often resistant to increased heavy atom concentrations. The continued lack of heavy atom binding was a surprising result, possibly due to the fact that the glutamate residues were involved in crystal contacts and thus not accessible for heavy atom binding.

Continued lack of success with crystal soaking prompted attempts to covalently modify rmHPLC6 prior to crystallization to ensure heavy atom incorporation. As outlined in Sections 4.3.3 and 4.3.4, rmHPLC6 AFP was successfully iodinated in solution and also overexpressed in the presence of seleno-L-methionine. By isolating homogeneous samples of I-HPLC6 and Se-HPLC6 prior to crystallization, we were certain that the resulting crystals each exhibited 100% heavy atom incorporation. However due to the small size of the HPLC6 protein, heavy atom incorporation induced the growth of non-isomorphous I-HPLC6 crystals with slightly altered packing arrangements. The I-rmHPLC6 crystallized in the  $\text{P}2_12_12_1$  space group with four molecules per asymmetric unit, whereas rmHPLC6 crystals ( $\text{C}222_1$ ) contained two molecules per asymmetric unit (Table 4.1). This encouraged optimization of the data collection conditions in hopes of exploiting the iodine

anomalous signal as a means to solve the structure using data from only a single I-rmHPLC6 crystal (Chen *et al.*, 1991).

Our first priority was to optimize data collection via the use of cryocrystallographic techniques because data collection at cryogenic temperatures serves to minimize crystal decay by drastically slowing the propagation of free radicals in frozen crystals. Rather than freezing crystals via insertion into the nitrogen cold stream (Section 4.4), a new system was developed which allowed crystals to be frozen by direct immersion into liquid nitrogen. This method provided increased heat transfer and therefore reduced crystal damage during the freezing process. Direct immersion into liquid nitrogen also provided the opportunity to stockpile frozen crystals in a storage dewar in order to maximize use of the data collection system. An improved box was constructed to enclose the collimator, nitrogen stream, goniometer head and detector surface (Figure 4.9). Made from plexiglass, the apparatus offered increased durability in comparison with the more flexible previous structure (Section 4.4). Secondly, the accumulation of frost on crystals during lengthy periods of data collection was eliminated by the new box. Complete data sets were therefore able to be collected on single crystals, thus improving overall data quality by eliminating the need to merge many data sets.

Next, the alignment of our x-ray system was examined to ensure that the incident x-ray beam was exactly orthogonal to the crystal oscillation axis. This correction facilitated the collection of Friedel pairs on the same data frame and thus contributed to significantly improving the overall quality of any anomalous signal. Having optimized the data collection system, a “fine-sliced” data set was collected on a single I-rmHPLC6

crystal at cryogenic temperatures over a period of four days with 15 minute frames per 0.25° oscillation.

In summary, the cloning, expression, iodination and crystallization of I-rmHPLC6 has provided our laboratory with a derivatized type III AFP from ocean pout suitable for x-ray analysis. Several methods were implemented to optimize our data collection system in order to maximize the quality of any iodine anomalous signal present in the x-ray data. It is hoped that careful processing of the recently-collected data will yield the much sought after crystal structure of a type III AFP followed by the proposal of a general mechanism by which proteins interact with ice.

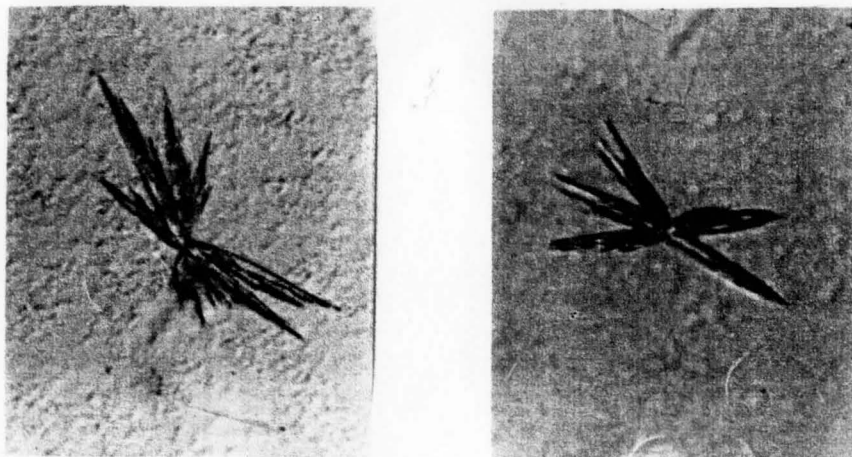


**Figure 4.1: Initial crystals of rmHPLC6.** Using Hampton Crystal Screen 2.48 (0.2 M ammonium phosphate; 0.1 M Tris-HCl pH 8.5; 50% v/v MPD), crystal clusters appeared overnight at 4°C and reached maximum size in less than a week (maximum spine length of 0.1 mm).

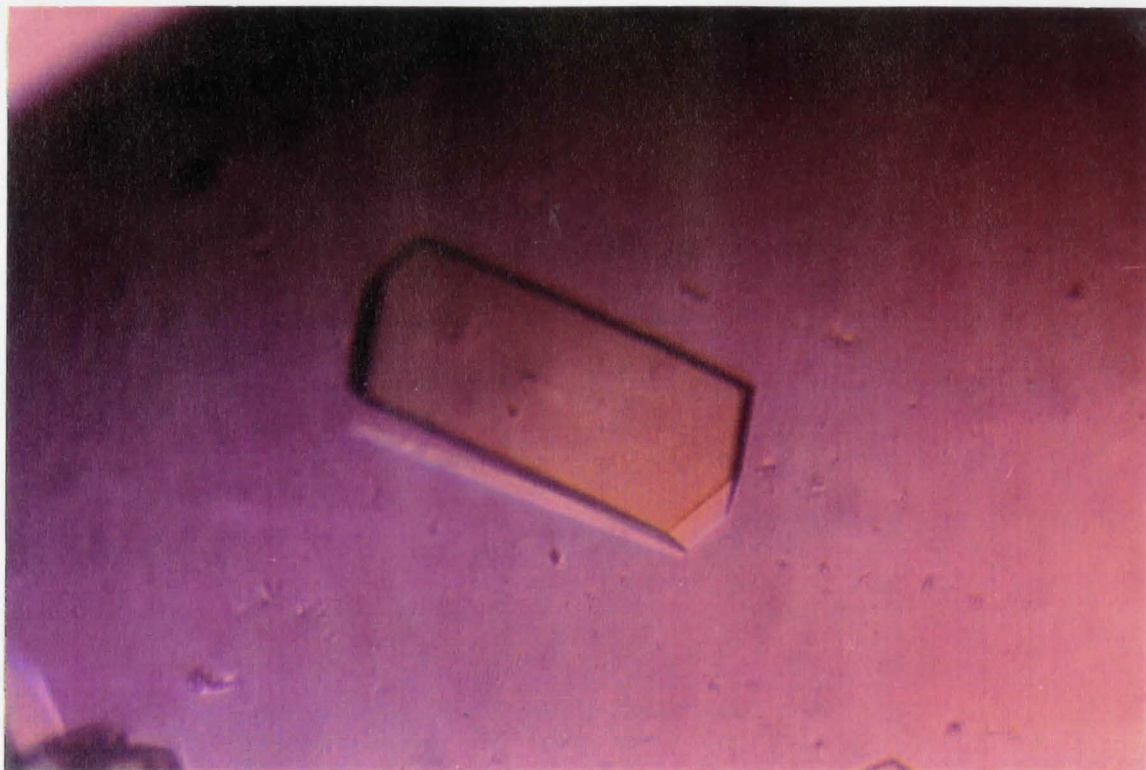


**Figure 4.2: Diffraction quality crystal of rmHPLC6.** Using a variation of Hampton Crystal Screen 1.04 (0.068 M Tris-HCl pH 8.0; 2.72 M ammonium sulfate), diffraction quality rmHPLC6 crystals (1.2 x 0.57 x 0.15 mm) were grown in three days at room temperature.

	-1	5	10	15	20	25	30	35	40	45	50	55	60	65			
(a)		QSV	VATQL	IPINT	ALTPA	MMEGK	VTNPI	GIPFA	EMSQI	VGKQV	NTPVA	KGQTL	MPNMV	KTYVA	G (65)		
(b)	<b>MGSSHHHHHSSGL</b>	<u>VPRGSH</u>	MKQSV	VATQL	IPINT	ALTPA	MMEGK	VTNPI	GIPFA	EMSQI	VGKQV	NTPVA	KGQTL	MPNMV	KTYVA	GK (88)	
(c)		<b>GSH</b>	MKQSV	VATQL	IPINT	ALTPA	MMEGK	VTNPI	GIPFA	EMSQI	VGKQV	NTPVA	KGQTL	MPNMV	KTYVA	GK (71)	
(d)	<b>MGSSHHHHHSSGL</b>	<u>VPRGSH</u>	<b>MDDDDK</b>	QSV	VATQL	IPINT	ALTPA	MMEGK	VTNPI	GIPFA	EMSQI	VGKQV	NTPVA	KGQTL	MPNMV	KTYVA	G (91)
(e)		QSV	VATQL	IPINT	ALTPA	MMEGK	VTNPI	GIPFA	EMSQI	VGKQV	NTPVA	KGQTL	MPNMV	KTYVA	G (65)		

**Figure 4.3: Amino acid sequences of HPLC6, rmHPLC6 and eHPLC6.** Residues are numbered relative to rHPLC6 (Li, Trinh & Hew, 1991) as in Figure 3.1. The length of each protein (# residues) follows each sequence. KEY: *His-tag*; thrombin cleavage sequence; enterokinase cleavage sequence; extra residues relative to the native HPLC6 are **bold**. (a) Native HPLC6 found in ocean pout sera. (b) His-rHPLC6. (c) rmHPLC6 final product. (d) His-eHPLC6. (e) Expected HPLC6 enterokinase cleavage product.

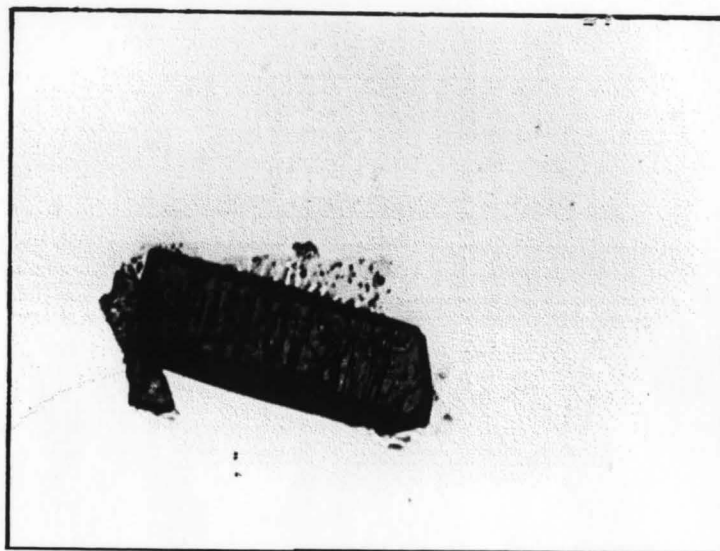


**Figure 4.4:** A damaged rmHPLC6 crystal. Crystals cracked in the presence of sufficiently high concentrations of heavy atom compounds, indicating a disturbance of the crystal packing. rmHPLC6 crystals were subsequently cross-linked with gluteraldehyde in order to increase crystal stability.

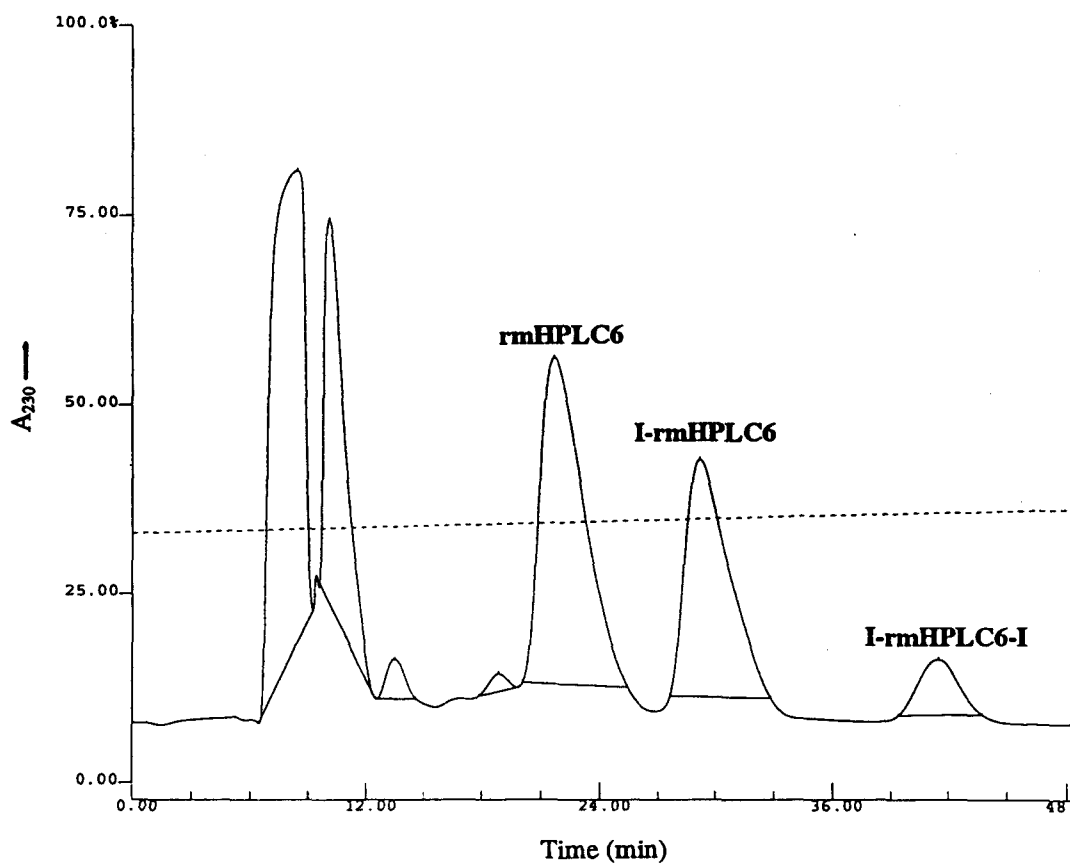


**Figure 4.5: Reverse phase purification of iodinated rmHPLC6.** Unreacted, mono-iodinated, and di-iodinated rmHPLC6 products are shown as they elute from a Waters  $\mu$ Bondapak C18 column (7.8 mm x 30 cm) using 0.1% trifluoroacetic acid and a 1 ml/min gradient of 33% to 36% acetonitrile over 50 minutes.

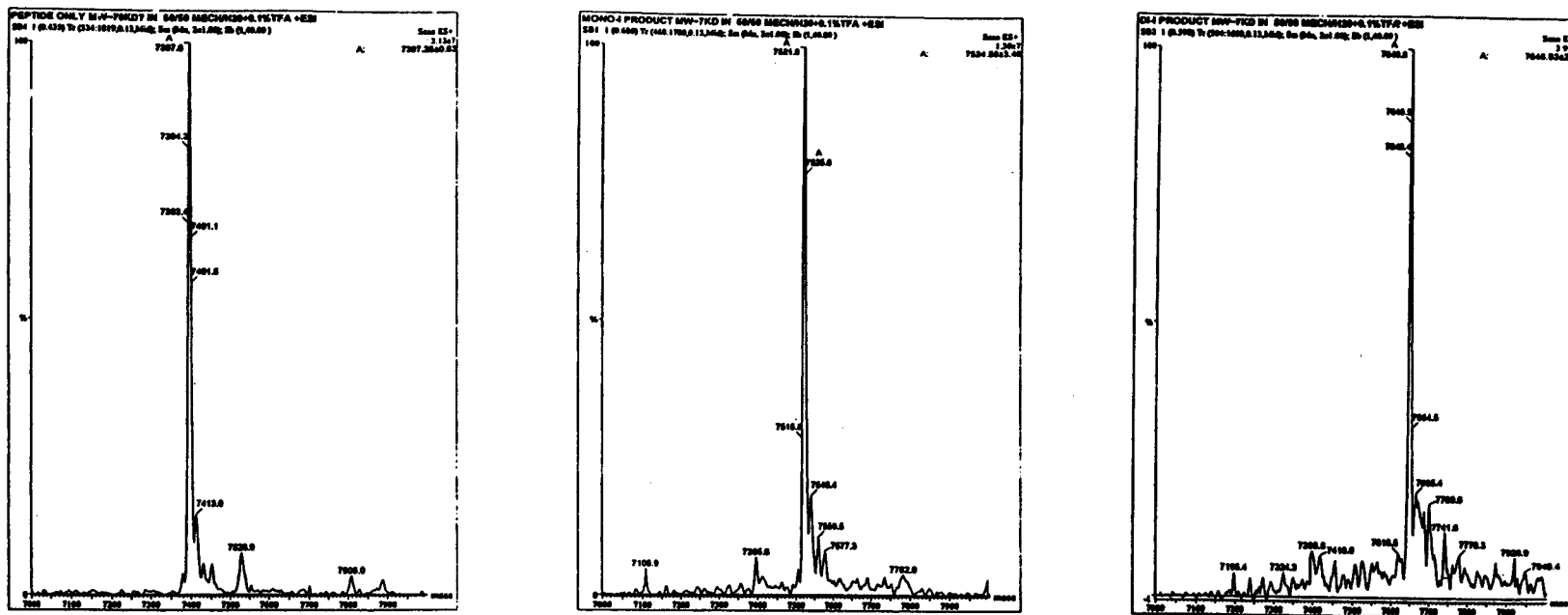


**Figure 4.6: Mass spectral profiles of rmHPLC6 iodination products.** Mono-iodinated (Middle: 7525 Da) and di-iodinated (Right: 7649 Da) products differ from unreacted rmHPLC6 (Left: 7397 Da) by the approximate mass of one and two iodine atoms respectively.



**Figure 4.7: Crystals of mono-iodinated rmHPLC6.** Crystals were grown using 0.068 M Tris-HCl pH 8.0 with 2.72 M ammonium sulfate. Once growth was initiated via seeding, crystals attained maximum size over a week at room temperature. Crystals of various sizes grew together in clusters, with the largest crystals having approximate dimensions of 1.0 x 0.4 x 0.2 mm.

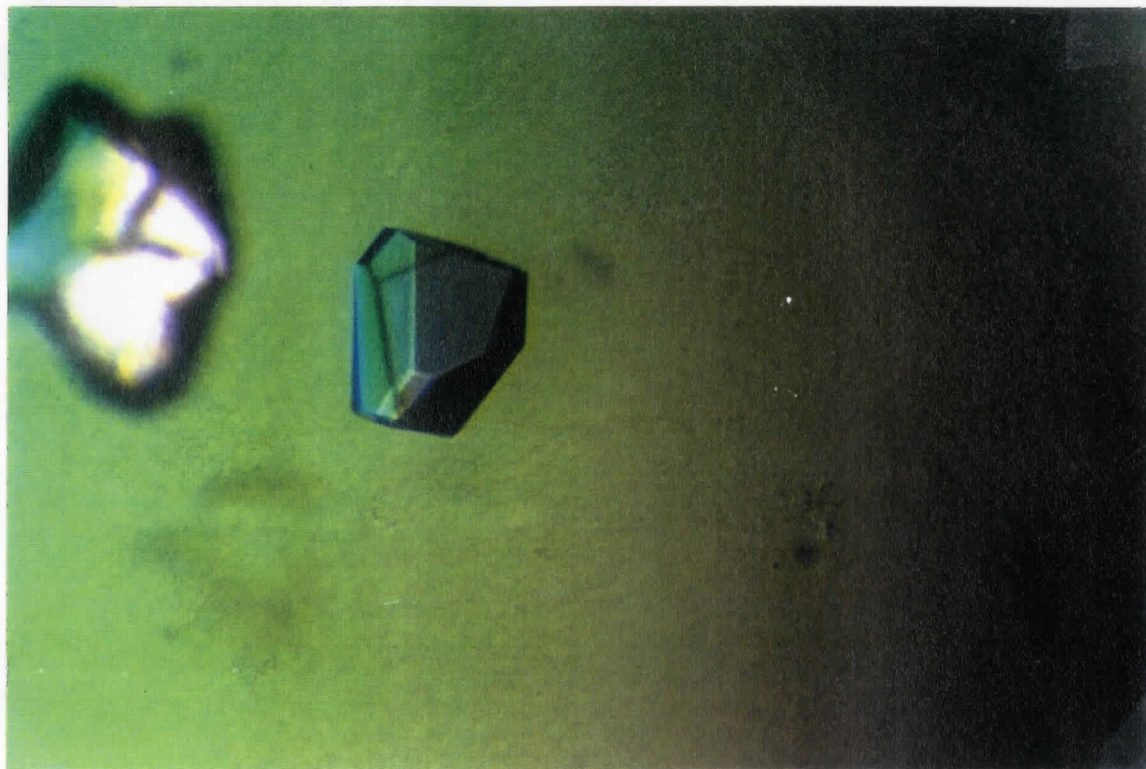


**Figure 4.8: Crystals of selenomethionyl rmHPLC6.** A lack of pure Se-rmHPLC6 limited the scope of crystallization trials available. The resulting few diffraction quality crystals (approx. 0.1 x 0.1 x 0.1 mm) were generated from crystallization conditions similar to those used for I-rmHPLC6 (Figure 4.7). Crystals achieved maximum size over two weeks at room temperature.

**Table 4.1: Data collection summary:** Performed on a RAXIS IIC area detector with CuK $\alpha$  radiation from a Rigaku RU200 rotating anode generator operating at 3kW (60mA x 50kV) with SUPPER double focusing mirrors and a 0.2mm focal spot.

Crystal	Peak1*	Peak1	Peak1	rmHPLC6	rmHPLC6	I-rmHPLC6
Temp.	RT	-165°C	-165°C	RT	-165°C	-165°C
Cryo-protectant		45% PEG	45% PEG		15% glycerol	15% glycerol
Mosaicity	0.2	1.1	1.4	0.20°	0.53°	0.52°
Space Group	P2 <sub>1</sub>	P2 <sub>1</sub>	P2 <sub>1</sub>	C222 <sub>1</sub>	C222 <sub>1</sub>	P2 <sub>1</sub> 2 <sub>1</sub> 2 <sub>1</sub>
# mol/A.U.	2	1	2	2	2	4
a (Å)	39.8	23.1	39.6	77.2	75.5	35.8
b (Å)	58.5	40.8	57.9	110.2	107.7	75.0
c (Å)	30.3	30.0	29.6	37.9	38.1	108.9
$\beta$	102.3°	100.6°	103.3°	90.0°	90.0°	90.0°
I/ $\sigma \geq 3$ (Å)	2.5	2.0	2.0	2.5	2.2	2.3
Complete	80.0 %	95.7 %	98.8 %	96.4 %	93.0 %	97.1 %
R-sym	7.0 %	8.0 %	8.6 %	4.5 %	4.4 %	5.6 %

\*(Xue *et al.*, 1994)

The “# mol/A.U.” represents the number of protein molecules per asymmetric unit. The “I/ $\sigma \geq 3$ ” indicates the resolution at which the average peak intensity is 3 times greater than the average error. Rsym is a measure of the agreement between equivalent reflections within a single data set (See Glossary).

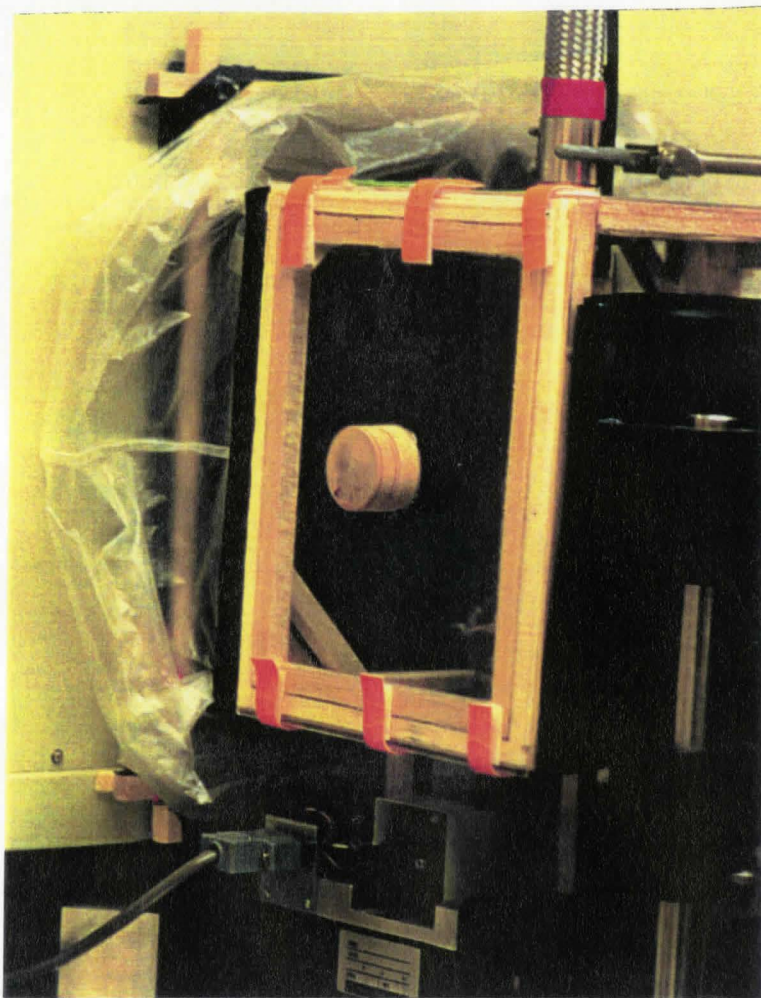


**Figure 4.9: Modified “cryo box”.** The plexiglass box was constructed to enclose the collimator, nitrogen stream, goniometer head, and detector surface in order to prevent contact with outside air and thus, eliminate frost accumulation on the crystal.

## **CHAPTER FIVE:**

---

### **CONCLUSION**

---

As a continuation of the work presented here, Yang *et al.* (1996) have used the Iterative Single Anomalous Scattering method (Wang, 1995) to solve the x-ray crystal structure of I-rmHPLC6 to 3.0 Å. Molecular replacement techniques were then used to solve the structure of the native ocean pout type III HPLC3 AFP to 2 Å (Figure 5.1). The increased resolution offered in comparison with the previous NMR structure (Sonnichsen *et al.*, 1993) has revealed a novel “pretzel fold.” This structural region has been statistically evaluated to exhibit a high degree of flatness and has been proposed to form the ice binding surface of the protein (Yang *et al.*, 1996). These findings reinforce an earlier proposal, based on type I AFPs, that a flat and rigid surface is essential to ice binding activity (Sicheri & Yang, 1995). Further studies are awaited to confirm if this theory in fact represents the general mechanism by which proteins interact with ice.

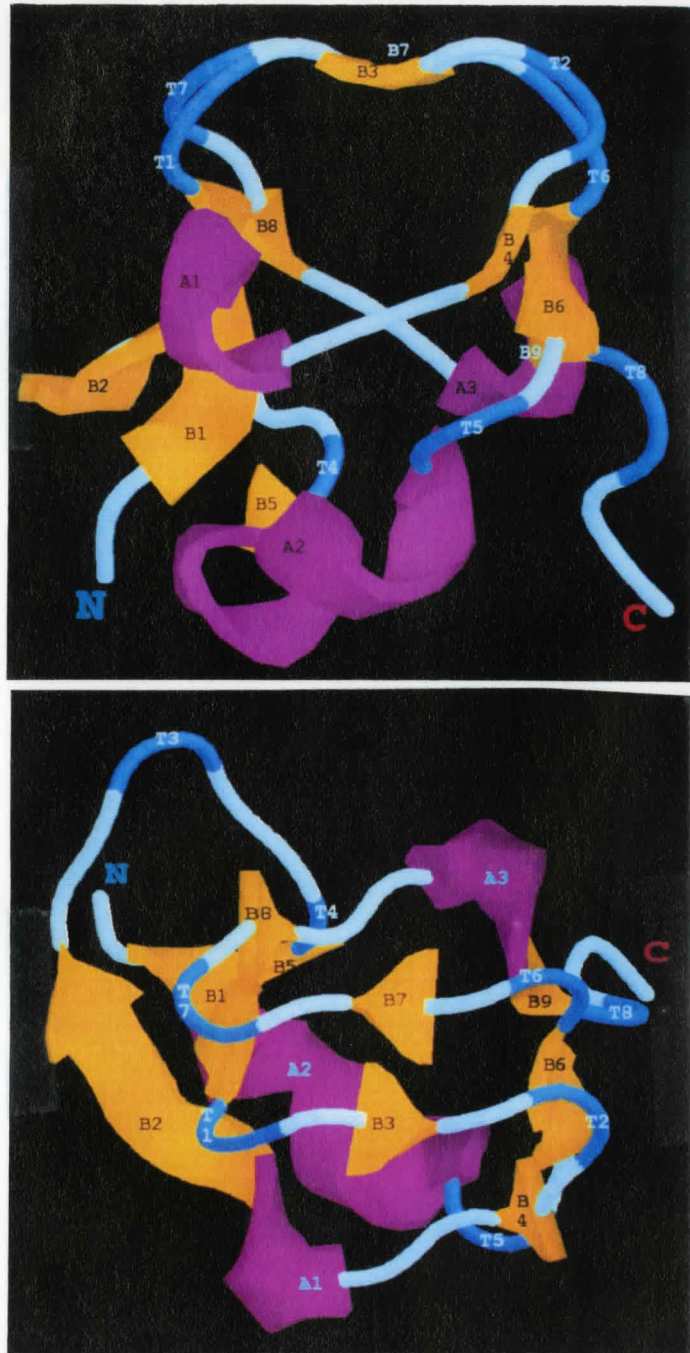


**Figure 5.1:** 2.0 Å X-ray crystal structure of a type III AFP from ocean pout. The “pretzel fold” is illustrated via two views: (top) top of photo; (bottom) coming out of the page. Secondary structures are as follows: pink:helix; yellow: $\beta$ -structure; blue: $\beta$ -turn. Reproduced from Yang *et al.*, 1996.

---

## GLOSSARY

---

**$R_{\text{merge}}$** : a measure of the agreement between two data sets

$$R_{\text{merge}} = \frac{\sum_{hkl} \sum_{j=1}^N ||F_{hkl}| - |F_{hkl}(j)||}{\sum_{hkl} N \times |F_{hkl}|}$$

**$R_{\text{sym}}$** : a measure of the agreement between symmetry-related reflections within a data set

$$R_{\text{sym}}(F) = \frac{\sum_{hkl} \sum_i ||F_i(h \ k \ l)| - |\overline{F(h \ k \ l)}||}{\sum_{hkl} \sum_i |F_i(h \ k \ l)|}$$

Equations were reproduced from Drenth, J., 1994.

---

## REFERENCES

---

Ananthanarayanan, V.S. (1989). Antifreeze proteins: structural diversity and mechanism of action. *Life Chem. Rep.* **7**: 1-31.

Ananthanarayanan, V.S., and Hew, C.L. (1977). Structural studies on the freezing point-depressing protein of the winter flounder. *Biochem. Biophys. Res. Commun.* **74**, 685-689.

Ausubel, F.M., Brent, R., Kingston, R.E., Moore, D.D., Siedman, J.G., Smith, J.A., and Struhl, K. (1993). *Current Protocols in Molecular Biology*. Current Protocols.

Brown, R.A., Yeh, Y., Burcham, T.S., and Feeney, R.E. (1985). Direct evidence for antifreeze glycoprotein adsorption onto an ice surface. *Biopolymers.* **24**: 1265-1270.

Burcham, T.S., Osuga, D.T., Yeh, Y., and Feeney, R.E. (1986). A kinetic description of antifreeze glycoprotein activity. *J. Biol. Chem.* **261**: 6390-6397.

Bush, C.A., and Feeney, R.E. (1986). Conformation of the glycotriptide repeating unit of antifreeze glycoprotein of polar fish as determined from the fully assigned proton n.m.r. spectrum. *Int. J. Pept. Protein. Res.* **28**: 386-397.

Bush, A., Feeney, R.E., Osuga, D.T., Ralapati, S., and Yeh, Y. (1981). Antifreeze glycoprotein. *J. Peptide Prot. Res.* **17**: 125-129.

Chao, H., Davies, P.L., Sykes, B.D., and Sonnichsen, F.D. (1993). Use of proline mutants to help solve the NMR solution structure of type III antifreeze protein. *Protein Sci.* **2**: 1411-1428.

Chao, H., DeLuca, C.I., and Davies, P.L. (1995) Mixing antifreeze protein types changes ice crystal morphology without affecting antifreeze activity. *FEBS Letters.* **357**: 183-186.

Chao, H., Sonnichsen, F.D., DeLuca, C.I., Sykes, B.D., and Davies, P.L. (1994). Structure-function relationship in the globular type III antifreeze protein: identification of a cluster of surface residues required for binding to ice. *Protein Sci.* **3**: 1760-1769.

Chen, L., Rose, J.P., Breslow, E., Yang, D.S.C., Chang, W.R., Fruey, W.F., Sax, M., and Wang, B.C. (1991). Crystal structure of a bovine neurophysin II dipeptide complex at 2.8Å determined from the single-wavelength anomalous scattering signal of an incorporated iodine atom. *Proc. Natl. Acad. Sci. USA.* **88**: 4240-4244.

Cheng, C.H.C, and DeVries, A.L. (1989). Structure of antifreeze peptides from the Antarctic eel pout, *Austrolycichthys brachycephalus*. *Biochim. Biophys. Acta.* **997**: 55-64.

Davies, P.L., and Hew, C.L. (1990). Biochemistry of fish antifreeze proteins. *FASEB J.* **4**: 2460-2468.

DeVries, A.L. (1971). Glycoproteins as biological antifreeze agents in antarctic fishes. *Science.* **172**: 1152-55.

DeVries, A.L. (1983). Antifreeze peptides and glycopeptides in cold water fishes. *Ann. Rev. Physiol.* **45**: 245-260.

DeVries, A.L. (1984). Role of glycopeptides and peptides in inhibition of crystallization of water in polar fishes. *Phil. Trans. R. Soc. London.* **B 304**, 575-588.

DeVries, A.L., Komatsu, S.K., and Feeney, R.E. (1970). Chemical and physical properties of freezing-point depressing glycoproteins from Antarctic fishes. *J. Biol. Chem.* **245**: 2901-2908.

DeVries, A.L., and Wohlschlag, D.E. (1969). Freezing resistance in some Antarctic fishes. *Science.* **163**: 1073-1075.

Drenth, J. (1994). *Principles of protein x-ray crystallography.* Springer-Verlag, New York. pp. 286.

Duman, J.G., and DeVries, A.L. (1976). Isolation, characterization, and physical properties of protein antifreezes from the winter flounder, *Pseudopleuronectes americanus*. *Comp. Biochem. Physiol.* **53B**, 375-380.

Ewart, V.K., and Fletcher, G.L. (1993). Herring antifreeze protein: primary structure and evidence for a C-type lectin evolutionary origin. *Mol. Mar. Biol. Biotechnol.* **2**: 20-27.

Ewart, V.K., and Fletcher, G.L. (1990). Isolation and characterization of antifreeze proteins from smelt (*Osmerus mordax*) and Atlantic herring (*Clupea harengus harengus*). *Can. J. Zool.* **68**: 1652-1658.

Ewart, V.K., Rubinsky, B., and Fletcher, G.L. (1992). Structural and functional similarity between fish antifreeze protein and calcium dependent lectins. *Biochem Biophys Res. Comm.* **185**: 1652-1658.

Feeney, R.E., Burcham, T.S., and Yeh, Y. (1986). Antifreeze glycoproteins from polar fish blood. *Ann. Rev. Biophys. Biophys. Chem.* **15**: 59-78.

Feeney, R.E., and Hofmann, R. (1973). Depression of freezing point by glycoproteins from an Antarctic fish. *Nature.* **243**: 357-359.

Feeney, R.E., and Yeh, Y. (1978). Antifreeze proteins from fish bloods. *Adv. Protein Chem.* **32**: 191-282.

Fletcher, N. (1970). *The chemical physics of ice*. Cambridge University Press, Cambridge. pp. 73-103.

Fletcher, G.L. (1977). Circannual cycles of blood plasma freezing point and Na<sup>+</sup> and Cl<sup>-</sup> concentrations in Newfoundland winter flounder (*Pseudopleuronectes americanus*): correlation with water temperature and photoperiod. *Can. J. Zool.* **55**: 789-795.

Franks, F., and Morris, E.R. (1978). Blood glycoprotein from Antarctic fish. *Biochem. Biophys. Acta.* **540**: 346-356.

Furey, W., and Swaminathan, S. (1990). *American Crystallographic Association Meeting Abstracts*. New Orleans, LA. PA33.

Graber, P., Bernard, A.R., Hassell, A.M., Milburn, M.V., Jordan, S.R., Proudfoot, A.E.I., Fattah, D., and Wells, T.N.C. (1993). Purification, characterisation and crystallisation of selenomethionyl recombinant human interleukin-5 from *Escherichia coli*. *Eur. J. Biochem.* **212**: 751-755.

Graves, B.J., Crowther, R.L., Chardran, C., Rumberger, J.M., Li, S., Huang, K.S., Presky, D.H., Familletti, P.C., Wolitzky, B.A., and Burns, D.K. (1994). Insight into E-selectin/ligand interaction from the crystal structure and mutagenesis of the lec/EGF domains. *Nature.* **367**: 532-538.

Harrison, K., Hallett, J., Burcham, T.S., Feeney, R.E., Kerr, W.L., and Yeh, Y. (1987). Ice growth in supercooled solutions of antifreeze glycoprotein. *Nature.* **328**: 241-243.

Hew, C.L., Fletcher, G.L., and Ananthanarayanan, V.S. (1980). Antifreeze proteins from the shorthorn sculpin, *Myoxocephalus scorpius*: isolation and characterization. *Can. J. Biochem.* **58**: 377-383.

Hew, C.L., Kao, M.H., So, Y.S., and Lim, K.P. (1983). Presence of cystine-containing antifreeze proteins in the Spruce budworm, *Choristoneura fumiferana*. *Can. J. Zool.* **61**: 2324-2328.

Hew, C.L., Slaughter, D., Fletcher, G.L., and Joshi, S.B. (1981). Antifreeze glycoproteins in the plasma of Newfoundland Atlantic cod (*Gadus morhua*). *Can. J. Zool.* **59**: 2186-2192.

Hew, C.L., Slaughter, D., Joshi, S.B., Fletcher, G.L., and Ananthanarayanan, V.S. (1984). Antifreeze polypeptides from the Newfoundland ocean pout, *Macrozoarces americanus*: presence of multiple and compositionally diverse components. *J. Comp. Physiol. Biochem. Syst. Environ. Physiol.* **155**: 81-88.

Hew, C.L., Wang, N.C., Joshi, S.B., Fletcher, G.L., Scott, G.K., Hayes, P.H., Buettner, B., and Davies, P.L. (1988). Multiple genes provide the basis for antifreeze protein diversity and dosage in the ocean pout. *J. Biol. Chem.* **263**: 12049-12055.

Hew, C.L., and Yang, D.S.C. (1992). Protein interaction with ice. *Eur. J. Biochem.* **203**: 33-42.

Hobbs, P.V. (1974). *Ice Physics*. Clarendon Press, Oxford.

Holden, H.M., and Rayment, I. (1991). Trimethyllead acetate: a first choice heavy atom derivative for protein crystallography. *Arch. Biochem. Biophys.* **291**: 187-194.

Holmes, W.N., and Donaldson, E.M. (1969). The body compartments and distribution of electrolytes. In *Fish Physiology* (Hoar, W.S., and Randall, D.J., eds). Academic Press, New York. pp. 1-89.

Jancariak, J., and Kim, S.H. (1991). Sparse matrix sampling: a screening method for crystallization of proteins. *J. Appl. Cryst.* **24**: 409-411.

Knight, C.A., Cheng, C.C., and DeVries, A.L. (1991). Adsorption of  $\alpha$ -helical antifreeze peptides on specific ice crystal surface planes. *Biophys. J.* **59**: 409-418

Knight, C.A., and DeVries, A.L. (1989). Melting inhibition and superheating of ice by and antifreeze glycopeptide. *Science.* **245**: 505-507.

Knight, C.A., DeVries, A.L., and Oolman, L.D. (1984). Fish antifreeze protein and the freezing and recrystallization of ice. *Nature.* **308**: 295-296.

Knight, C.A., Driggers, E., and DeVries, A.L. (1993). Adsorption to ice of fish antifreeze glycopeptides 7 and 8. *Biophys. J.* **64**: 252-259.

Li, X.M., and Hew, C.L. Structure and function of an antifreeze polypeptide from ocean pout, *Macrozoarces americanus*: role of glutamic acid residues in protein stability and antifreeze activity by site-directed mutagenesis. *Protein Engineering.* **4**, 1003-1008.

Li, X.M., Trinh, K.Y., and Hew, C.L. (1991). Expression and characterization of an active and thermally more stable recombinant antifreeze polypeptide from ocean pout, *Macrozoarces americanus*, in *Escherichia coli*: improved expression by the modification of the secondary structure of the mRNA. *Protein Engineering*. **4**, 995-1002.

Li, X.M., Trinh, K.Y., Hew, C.L., Buettner, B., Baenziger, J., and Davies, P.L. (1985). Structure of an antifreeze polypeptide and its precursor from the ocean pout, *Macrozoarces americanus*. *J. Biol. Chem.* **260**: 12904-12909.

Matthews, B.W. (1985). Determination of protein molecular weight, hydration, and packing from crystal density. In *Methods in Enzymology*. (Wyckoff, H.A., Hirs, C.H.W., and Timasheff, S.N., eds) Academic Press, Inc., Toronto, ON. pp. 176-187.

Means, G.E., and Feeney, R.E. (1971). *Chemical Modifications of Proteins*. Holden-Day, Inc., San Francisco, CA.

*New England Biolabs 1993-94 Catalog*. (1993). New England Biolabs. Beverly, MA.

Ng, N.F., and Hew, C.L. (1992). Structure of an antifreeze polypeptide from sea raven. *J. Biol. Chem.* **267**: 16069-16075.

Ng, N.F., Trinh, K.Y., and Hew, C.L. (1986). Structure of an antifreeze polypeptide precursor from the sea raven. *J. Biol. Chem.* **261**: 15690-15695.

Otwinowski, Z. (1993). DENZO, oscillation data reduction program. *In Proceedings of the CCP4 study weekend: "Data collection and processing." January 29-30.* Compiled by: Sawyer, L., Isaacs, N., and Bailey, S. SERC Daresbury Laboratory, England. pp. 55-62.

Patterson, J.L., and Duman, J.G. (1982). Purification and composition of insect antifreezes with high cysteine contents from the larvae of the beetle, *Tenebrio molitor*. *J. Exp. Zool.* **219**, 381-384.

Petsko, G.A. (1985). Preparation of isomorphous heavy-atom derivatives. *In Methods in Enzymology.* (Wyckoff, H.A., Hirs, C.H.W., and Timasheff, S.N., eds) Academic Press, Inc., Toronto, ON. **115**: 147-156.

Rao, B.N.N., and Bush, C.A. (1987). Comparison by  $^1\text{H-NMR}$  spectroscopy of the conformation of the 2600 Dalton antifreeze glycopeptide of polar cod with that of high molecular weight antifreeze glycoprotein. *Biopolymers.* **26**: 1227-1244.

Raymond, J.A., and DeVries, A.L. (1972). Freezing behaviour of fish blood glycoproteins with antifreeze properties. *Cryobiology.* **9**: 541-547.

Raymond, J.A., and DeVries, A.L. (1977). Adsorption inhibition as a mechanism of freezing resistance in polar fishes. *Proc. Natl. Acad. Sci. USA.* **74**: 2589-93.

Schneppenheim, R., and Theede, M. (1980). Isolation and characterization of freezing point depressing peptides from larvae of *Tenebrio molitor*. *Comp. Biochem. Physiol.* **67B**: 561-568.

Scholander, P.F., and Maggert, J.E. (1971). Supercooling and ice propagation in blood from arctic fish. *Cryobiology.* **8**: 371-74.

Scholander, P.F., Vandam, L., Kanwisher, J.W., Hammel, H.T., and Gordon, M.S. (1957). Supercooling and osmoregulation in Arctic fish. *J. Cell. Comp. Physiol.* **49**: 5-24.

Schrag, J.D., Cheng, C.H.C., Panico, M., Morris, H.R., and DeVries, A.L. (1987). Primary and secondary structure of antifreeze peptides from Arctic and Antarctic zoarcid fishes. *Biochim. Biophys. Acta.* **915**: 357-370.

Scott, G.K., Hayes, P.H., Fletcher, G.L., and Davies, P.L. (1988). Wolffish antifreeze protein genes are primarily organized as tandem repeats that each contain two genes in inverted orientation. *Mol. Cell. Biol.* **8**: 3670-3675.

Sicheri, F., and Yang, D.S.C. (1995). Ice-binding structure and mechanism of an antifreeze protein from winter flounder. *Nature.* **375**: 427-431.

Sigler, P.B. (1970). Iodination of a single tyrosine in crystals of  $\alpha$ -chymotrypsin. *Biochemistry.* **9**: 3609-3617.

Slaughter, D., Fletcher, G.L., Ananthanarayanan, V.S., and Hew, C.L. (1981).

Antifreeze proteins from the sea raven, *Hemirhamphys americanus*: further evidence for diversity among fish polypeptide antifreezes. *J. Biol. Chem.* **256**: 2022-2026.

Sonnichsen, F.D., Sykes, B.D, Chao, H., and Davies, P.L. (1993) The nonhelical structure of antifreeze protein type III. *Science.* **259**: 1154-1157.

Sonnichsen, F.D., Sykes, B.D., and Davies, P.L. (1995). Comparative modeling of the three-dimensional structure of Type II antifreeze protein. *Protein Science.* **4**:460-471.

Stura, E.A., and Chen, P. (1992). Soaking of crystals. In *Crystallization of Nucleic Acids and Proteins: A Practical Approach*. (Ducruix, A., and Giege, R., eds) Oxford University Press, New York, NY. pp. 241-253.

Stura, E.A., and Wilson, I.A. (1992). Seeding techniques. In *Crystallization of Nucleic Acids and Proteins: A Practical Approach*. (Ducruix, A., and Giege, R., eds) Oxford University Press, New York, NY. pp. 99-126.

Tomimatsu, Y., Scherer, J., Yeh, Y., and Feeney, R.E. (1976). Raman spectra of a solid antifreeze glycoprotein and its liquid and frozen aqueous solutions. *J. Biol. Chem.* **251**: 2290-2298.

Walter, R., Slaybaugh, M., and Ealick, S. (1995). *Cryocrystallography, the Application of Low Temperature Crystallographic Techniques: a Practical Approach (video)*.

©W.M. Keck Laboratory for Molecular Structure, Cornell University, NY.

- Wang, B.C. (1995). Resolution of phase ambiguity in macromolecular crystallography. In *Methods in Enzymology*. (Wyckoff, H.A., Hirs, C.H.W., and Timasheff, S.N., eds) Academic Press Inc., Toronto, ON. **115B**: 90-97.
- Wang, X., DeVries, A.L., and Cheng, C.H. (1995). Genomic basis for antifreeze peptide heterogeneity and abundance in an Antarctic eel pout: gene structures and organization. *Mol. Mar. Biol. Biotechnol.* **4**: 135-147.
- Weis, W.I., Drickamer, K., and Hendrickson, W.A. (1992). Structure of a C-type mannose-binding protein complexed with an oligosaccharide. *Nature.* **360**: 127-134.
- Weis, W.I., Kahn, R., Fourme, R., Drickamer, K., and Hendrickson, W.A. (1991). Structure of the calcium-dependent lectin domain from a rat mannose-binding protein determined by MAD phasing. *Science.* **254**: 1608-1615.
- Wen, D., and Laursen, R.A. (1992). A model for binding of an antifreeze polypeptide to ice. *Biophys. J.* **63**: 1659-1662.
- Wyckoff, H., Hirs, C.H.W., and Timasheff, S.N. (Eds.) (1985). *Methods of Enzymology*, Vol. 114 & 115. Academic Press Inc., Toronto.
- Xue, Y.Q., Sicheri, F., Ala, P., Hew, C.L., and Yang, D.S.C. (1994). Single crystals of a type III antifreeze polypeptide from ocean pout. *J. Mol. Biol.* **237**: 351-352.

Yang, D.S.C. (1993). Protein-ice interactions: antifreeze proteins. In *The Amphipathic Helix*. (Epanand, R.M., ed) CRC Press, Boca Raton, Fl. pp. 369-391.

Yang, D.S.C., Bubanko, S.A., Xue, Y.Q., Seethraman, J., Hew, C.L., and Sicheri, F. (1996). Flat and rigid ice-binding surface on a nonhelical antifreeze protein. Submitted to *Science*.

Yang, D.S.C., Sax, M., Chakrabarty, A., and Hew, C.L. (1988). Crystal structure of an antifreeze polypeptide and its mechanistic implications. *Nature*. **333**: 232-237.